SINTEF

Report No - Restricted

Atmospheric chemistry- Aqueous phase chemistry

Project 257430193: D6 Final report

Authors
Matthias Karl (NILU), Pierre Herckes (Arizona State University), William Mitch (Yale University) and Eirik Falck da Silva (SINTEF)

SINTEF Materials and Chemistry
Process Technology
2012-05-25

SINTEF

SINTEF Materialer og kjemi
SINTEF Materials and Chemistry

Address:
Postboks 4760 Sluppen
NO-7465 Trondheim
NORWAY

Telephone:+47 73593000
Telefax:+47 73597043

info.mk@sintef.no
www.sintef.no/mk
Enterprise /VAT No:
NO 948007029 MVA

Report

Project 257430193: D6 Final report

Subtitle

KEYWORDS:
Amine
Atmospheric chemistry
Nitrosamine

VERSION
2

DATE
2012-05-25

AUTHORS
Matthias Karl (NILU), Pierre Herckes (Arizona State University)
William Mitch (Yale University) and Eirik F. da Silva (SINTEF)

CLIENT(S)
CCM

CLIENT'S REF.
Arne Myhrvold

PROJECT NO.
801819

NUMBER OF PAGES/APPENDICES:
~~57~~ 58

ABSTRACT

This report summarizes the main findings of the atmospheric chemistry-aqueous phase chemistry project.

PREPARED BY
Eirik Falck da Silva

SIGNATURE

CHECKED BY
Torbjørn Pettersen

SIGNATURE

APPROVED BY
Webjørn Remen, Research Director

SIGNATURE

REPORT NO. ~~Report No.~~ SINTEF F23082
ISBN ISBN
CLASSIFICATION Restricted
CLASSIFICATION THIS PAGE Restricted

Document history

VERSION	DATE	VERSION DESCRIPTION
1	2012-04-27	Draft report submitted to CCM
2	2012-05-25	Final report after first review by CCM

SINTEF

Table of contents

1 Introduction

An amine-based CO_2 capture plant may cause harmful emissions to the atmosphere. Amines and degradation products from reactions in the process and in the atmosphere are of particular concern, but there is limited knowledge about the behaviour of these chemical compounds. Thus, several studies have been initiated by the CCM project to increase this knowledge. This study, making use of kinetic data from new experiments and advanced box modelling, aims to uncover the possible formation of nitrosamines and nitroamines by amines in the atmospheric aqueous phase of fog and clouds.

In addition to the reactions leading to the formation of nitrosamines and nitramines in the gas phase and aqueous phase, there may be important competing atmospheric reactions that can affect these processes. Any such reactions have been included in a box model description of the chemistry. Examples of such reactions are atmospheric oxidation of NO emitted with the plume and NO2 photolysis. Scenarios and initial chemical concentrations of atmospheric reactive constituents and typical meteorological parameters of the Mongstad region determined in WP2 ("Specification of the aqueous phase atmospheric conditions") will be used in the box model simulations.

The multiphase chemistry/aerosol box model MAFOR by Matthias Karl (NILU) was used to simulate a fog cycle similar to that described by Hutchings (2010). The aqueous phase chemistry of the selected amines of this study has been included in the model in addition to the atmospheric gas phase chemistry of amines and the tropospheric background chemistry in the gas phase and in the aqueous phase. The data from the literature study (WP3: "Aqueous phase nitrosamine and nitramine formation") was used to develop the aqueous phase chemistry module of amines for use in the box model.

The atmospheric gas phase mechanism for amine (amine + OH) has been based on previous mechanisms derived in the ADA ("Atmospheric Degradation of Amines") projects 2009/2010 (http://ada.nilu.no) and the compilation of kinetic data (experimental + QSAR predicted) prepared during Call-off 1. The mechanism for the aqueous phase chemistry was developed in this project. The aqueous phase reaction of amines with the aqueous hydroxyl radical (OHaq) were included in the model. This reaction will compete with other reactions of the amine in the aqueous phase and could be an important loss of amines in the aqueous phase, without forming nitrosamine/nitramines.

An updated box model was developed based on the outcome of the experiments (WP5: "Execution of experiments") and the importance of aqueous phase reactions be illustrated. Scenarios representing continental and marine air were simulated. Simulations of a 3-day period with a cycle of 3 full fog episodes were done. Model data from box model simulations that include the updated aqueous phase chemistry were analysed and the kinetics and product distribution in the aqueous phase and in the gas phase will be compared with gas phase (amine + OH) conditions.

Rate expressions and rate constants for implementation in the reactive dispersion model will be recommended for nitrosamine and nitramine formation from generic amines. The recommended expressions will be embedded in a detailed aqueous phase reaction scheme and it is out of the scope of WP6 to developed simplified expressions. The data for use in the reactive dispersion model will distinguish between primary, secondary and tertiary amines based on the series of ethanolamines and methylamines.

2 Scenario description

In the report from WP2 ("D1 - Specification of the aqueous phase atmospheric conditions") eight scenarios were created for use in box modelling; representing the Mongstad area in four different seasons (MAM, JJA, SON, DJF) when marine air mass arrived from either northwest (NNW, 270°-360°) or south-southeast (SEW, 120°-210°). All data is based on meteorological (measurements and modelled fields) and chemical data of the year 2007. The chemical composition of the aqueous phase of fogs was derived from the chemical analysis of rain water composition at Haukeland and Nausta, and the chemical analysis of fog samples collected near Oslo. Model scenarios were defined for a simulation time of 3 days (72 hours) with a fog cycle. Figure 1 shows the temperature profiles and Figure 2 shows the relative humidity profiles of the eight scenarios.

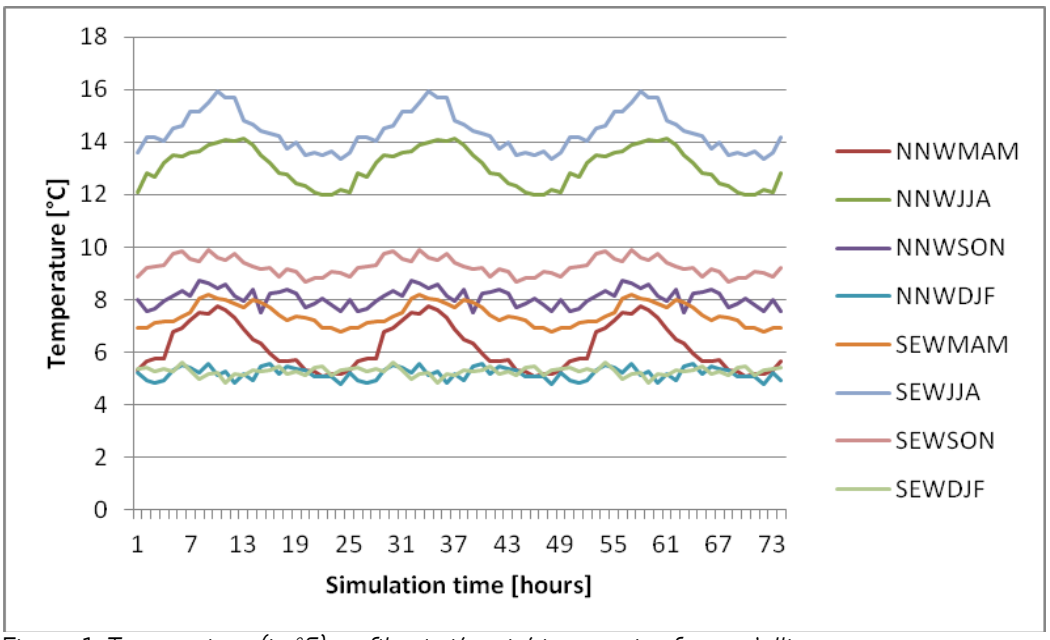

Figure 1: *Temperature (in °C) profiles in the eight scenarios for modelling.*

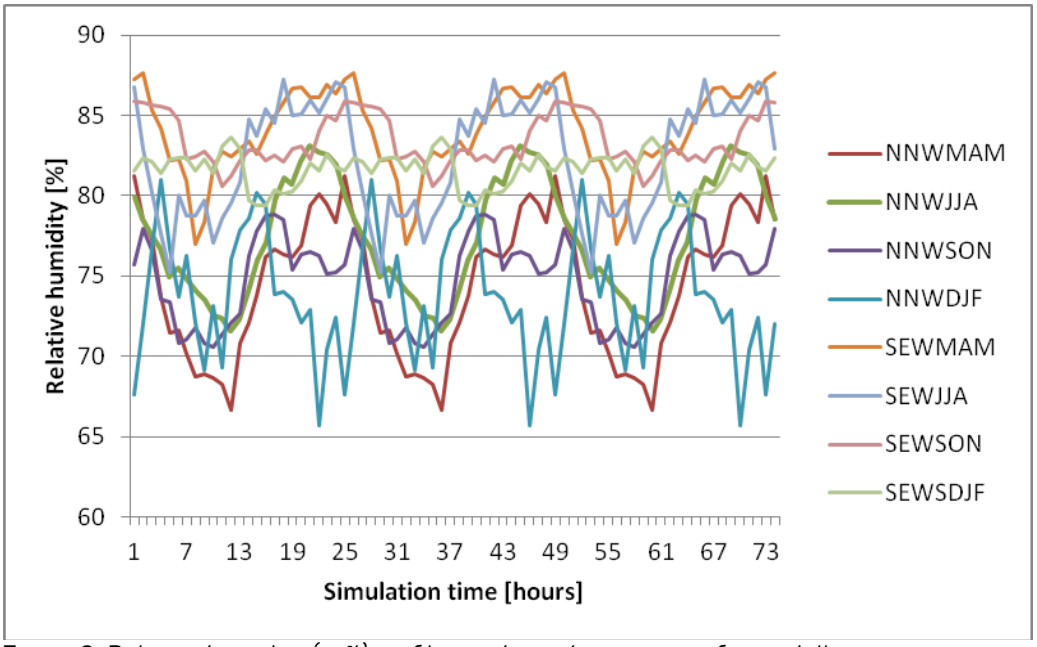

Figure 2: *Relative humidity (in %) profiles in the eight scenarios for modelling.*

Each fog event started at 2 a.m. and ended at 10 a.m. (8 hours). The fog cycle was prescribed to the model; fog formed at approximately 2 a.m. and fog dissipated at approximately 10 a.m. so that three full fog events were simulated. The fog cycle considered the maximum liquid water content, LWC_{max}, of clouds as derived from TAPM simulations (Karl et al., 2011a). The amplitude of LWC ranged from 9 mg m^{-3} to about 100 mg m^{-3} or 140 mg m^{-3}, depending on the LWC_{max} of the respective scenario. Relative humidity was set to 95% during the fog periods. Figure 3 shows the LWC profiles in the eight scenarios.

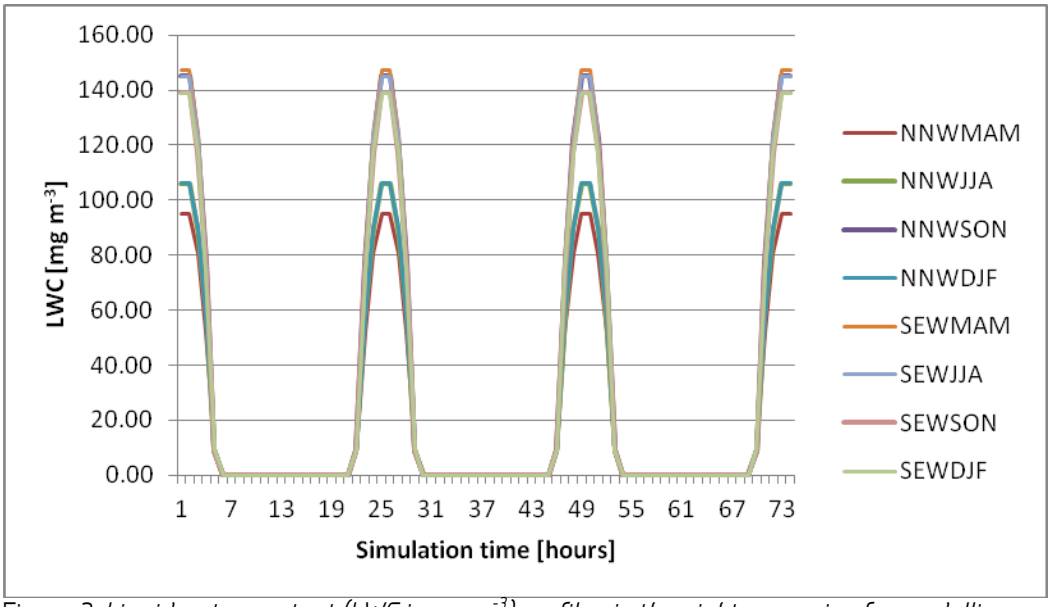

Figure 3: *Liquid water content (LWC in mg m^{-3}) profiles in the eight scenarios for modelling.*

Initial concentrations of gas phase constituents were the same in all model runs and are displayed in ***Table 1***.

Table 1: Initial concentration (in molecules cm^{-3}) of gas phase constituents in all model runs.

Species	molecules cm^{-3}
NO	1.20E+10
NO2	4.78E+10
O3	9.31E+11
CH4	4.42E+13
HCHO	2.60E+10
H2O2	1.30E+10
HONO	5.20E+09
DMS	2.60E+09
HCl	1.30E+10
CO	2.60E+12
CO2	8.58E+15
C2H6	9.36E+09
C2H4	9.36E+09
C3H8	9.36E+09
TOLUENE	3.90E+09
AMINE	6.50E+09

Emissions of atmospheric background compounds were added in all scenarios (see Table 2). The emission rates were chosen to represent a moderately polluted boundary layer of a coastal (marine) location. The boundary layer height was set to 1000 m in all runs. Emissions of amines were added in the model simulations that were made to represent realistic atmospheric scenarios at Mongstad. In the model runs for determination of the production yields of nitrosamines and nitroamines, no emissions of amines were introduced. The emission rate of all amines were estimated based on modelled maximum concentrations of MEA obtained in the worst case scenario calculations with TAPM (Karl et al., 2011a). The emission rate was identical for all amines.

Table 2: Emission rates (in molecules cm^{-2} s^{-1}) of gas phase constituents in all model runs.

DMS	6.00E+09
H2O2	4.00E+09
NO	7.00E+10
HCHO	5.50E+10
HONO	3.60E+10
CO	2.40E+11
C2H6	2.40E+10
C3H8	2.40E+10
C2H4	2.40E+10
TOLUENE	3.60E+09
AMINE	1.28E+10

Gaseous nitrous acid (HONO) is of special importance to this project; first because the photolysis of HONO is a significant source of hydroxyl (OH) radicals in the troposphere, and second because HONO in the aqueous phase is an important nitrosating agent. A homogenous gas phase reaction between secondary amines and HONO leading to formation of nitrosamines has been postulated by Hanst et al. (1977), but it was later demonstrated

that the nitrosamines formation takes place as a surface-catalyzed reaction on the surfaces of the experimental reactor (Glasson, 1979). A full discussion of this subject is given in the report from WP1 ("D1 - Evaluation of Atmospheric Chemistry Status overview").

Heterogeneous production of HONO in the troposphere may take place on aerosol surfaces or/and on ground surfaces such as buildings and vegetation surfaces (Aumont et al., 2003). Typical daytime concentrations of HONO in the atmospheric boundary layer of 50-150 pptv have been measured (Kleffmann et al., 2003). While a HONO source at ground is commonly required in order to explain ambient levels of HONO in the troposphere (Vogel et al., 2003) and despite its relevance as precursor for nitrosamines (Platt et al., 1980), no HONO measurements have been performed at Mongstad.

In urban areas it was found that HONO levels are closely related to ambient NO_2 levels (Figure 4). This is in agreement with laboratory studies suggesting that the heterogeneous reaction leading to HONO is first order in NO_2 (e.g. Finlayson-Pitts and Pitts, 2000 and references therein). Based on the tentative relationship shown in Figure 4, an ambient level of about 300 pptv HONO during nighttime was estimated for Mongstad (typical NO_2 levels at 2 ppbv on monthly average).

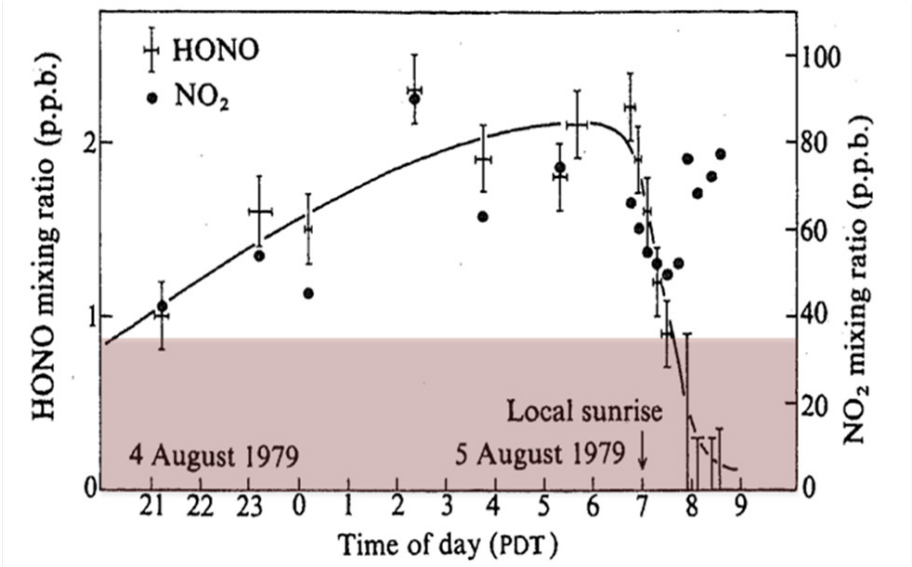

Figure 4: Diurnal concentration profiles of HONO (left y-axis) and NO_2 (right y-axis) based on measurements in August 1979 in Riverside, CA. Adopted from Platt et al. (1980). Shaded part indicates possible range of daily NO_2 concentrations measured at Mongstad.

The continuous emission rate of HONO in the model was adjusted to produce 300 pptv in the NNWJJA scenario. Modelled HONO levels in the SEWDJF were up to 1000 ppt.

Initial concentrations of constituents in the aqueous phase are summarized in Table 3. These concentrations were used to initialize the fog droplet composition in the model simulations that were made to represent realistic atmospheric scenarios at Mongstad

Table 3: Concentrations (in mol L_{H2O}^{-1}, short M) of aqueous phase constituents in all model runs.

	MAM	JJA	SON	DJF
Species	**M**	**M**	**M**	**M**
O_2(aq)	3.00E-04	3.00E-04	3.00E-04	3.00E-04
OH^-(aq)	1.58E-09	1.26E-09	2.00E-09	2.00E-09
Cl^-(aq)	6.57E-04	1.96E-04	6.03E-04	8.27E-04
Fe^{3+}(aq)	2.90E-07	2.90E-07	2.90E-07	2.90E-07
SO_4^{2-}(aq)	1.10E-05	1.20E-05	4.00E-06	4.00E-06
NH_4^+(aq)	6.30E-05	3.80E-05	2.00E-05	2.80E-05
HCO_3^-(aq)	7.04E-07	7.04E-07	7.04E-07	7.04E-07
NO_3^-(aq)	1.10E-05	1.20E-05	6.00E-06	8.00E-06
DOC(aq)	5.80E-05	5.80E-05	5.80E-05	5.80E-05
pH	5.2	5.1	5.3	5.3

Initial concentrations of Cl^-, SO_4^{2-}, NO_3^- and NH_4^+ in the fog droplets are based on measurements presented in the WP2 report. The concentrations of these ions vary for the four seasons. Initial concentration of the total dissolved organic carbon (DOC) was adopted from the average value found by Herckes et al. (2007). Initial concentration of Fe^{3+} was adopted from the average value of the total iron concentration at a coastal Pacific site reported by Siefert et al. (1998). Initial concentrations of all other compounds are taken from the marine scenario developed for the CAPRAM 2.4 model (Ervens et al., 2003).

2.1 Model description

2.1.1 Chemistry solver

The 0-dimensional Lagrangian type sectional aerosol box model, MAFOR (Marine Aerosol Formation) version 1.4, which includes gas phase and aqueous phase chemistry in addition to aerosol dynamics (Karl et al., 2011b; Karl et al., 2012), was used in this work. The basic tropospheric multiphase chemistry scheme of MAFOR is based on the Module Efficient Calculating the Chemistry of the Atmosphere (MECCA) (Sander et al., 2005; Sander et al., 2011) and includes halogen chemistry (Sander and Crutzen, 1996), chemistry of C_2-C_4 alkanes, propene, toluene and dimethyl sulphide (Karl et al., 2007). Chlorine chemistry was considered in the present work, while bromine and iodine chemistry were not considered. Gas phase chemistry of 2-aminoethanol (MEA), monomethylamine (MMA), dimethylamine (DMA), trimethylamine (TMA) has been added to the model during the ADA projects. Gas phase mechanisms of diethanolamine (DEA) and triethanolamine (TEA) were added in this work. DEA and TEA mechanisms are not very detailed and roughly follow the mechanism of MDEA outlined in the report by Bråthen et al. (2008). The reaction of amines with the chlorine atom were however not implemented, and oxidation of amines in the gas phase occurred only via reaction with the hydroxyl radical (OH). Details on the gas phase mechanism of amines is provided in chapter 1.3 and details on the aqueous phase mechanism of amines is provided in chapter 1.4.

Diurnal variations of photolysis rates are based on Landgraf and Crutzen (1998) using updated data on quantum yield and absorption cross-sections recommended by the Jet Propulsion Laboratory (JPL) Evaluation no. 15 (Sander et al., 2006). The kinetic pre-processor (KPP) solver package (http://people.cs.vt.edu/~asandu/Software/Kpp/) was used to generate Fortran95 code for the chemistry module and the Rosenbrock 3 solver was used for integration the differential equation system of gas phase reactions (Sandu et al., 1997; Sandu and Sander, 2006).

2.1.2 Multiphase chemistry

Henry's Law describes the equilibrium partitioning between gas phase and aqueous phase without any consideration of the time scales of the uptake process. However, Schwartz (1986) has shown that the uptake rate of gases to the droplet is a time dependent process which may be controlled by several factors, including gas phase diffusion, interfacial mass transfer, aqueous phase diffusion and chemical reactions within the aqueous phase. The reciprocal value of the rate (in s^{-1}) of each process can be defined as a characteristic time. A comparison of these characteristic times allows the determination of the rate-limiting process.

For most practical purposes, the uptake rate is only dependent on the rate of transport from the gas phase, which is determined by gas phase diffusion followed by interfacial mass transfer. This means, that it is assumed in this work that a) the time scale for the aqueous phase diffusion of amines is significantly shorter than that for the mass transfer from the gas phase and b) chemical reaction of amines (nitrosoamines, nitroamines, etc.) in the droplets is slow compared to aqueous phase diffusion. Both assumptions appear to be reasonable for the compound classes under investigation.

In a system with equilibrium partitioning of gas phase constituents to the aqueous phase of aerosols and clouds, the changes of gas phase and aqueous phase concentrations of compound *q* with time are described by:

$$\frac{dC_{g,q}}{dt} = Q_{g,q} - k_{m,q} LWC\left(C_{g,q} - \frac{C_{aq,q}}{H_q}\right) \quad (1a)$$

$$\frac{dC_{aq,q}}{dt} = Q_{aq,q} + k_{m,q}\left(C_{g,q} - \frac{C_{aq,q}}{H_q}\right) \quad (1b)$$

where $C_{g,q}$ and $C_{aq,q}$ are the gas phase and aqueous phase concentrations of compound q, respectively. Both concentrations are given in terms of gas phase units (i.e. cm^{-3}). $Q_{g,q}$ and $Q_{aq,q}$ are the respective gas phase and aqueous phase net production terms ($cm^{-3}\ s^{-1}$), LWC is liquid water content (m^3/m^3), H_q is the dimensionless Henry coefficient. The transfer of molecules from the gas phase to the aqueous phase and vice versa is treated by the resistance model of Schwartz (1986). The mass transfer coefficient, $k_{m,q}$, is a first order loss rate constant (in s^{-1}) that describes the mass transport of compound q from the gas phase to the aqueous phase and depends on the droplet's radius (Schwartz, 1986):

$$k_{m,c} = \left(\frac{r_d^2}{3D_q} + \frac{4r_d}{3c_{m,q}\alpha_q}\right)^{-1} \quad (2)$$

Where D_q is the gas phase diffusion coefficient (in $m^2\ s^{-1}$), $c_{m,q}$ is the molecular speed (in $m\ s^{-1}$) and α_q is the mass accommodation coefficient of compound q, and r_d is radius of the droplets.

It is assumed that the liquid aerosol behaves as an ideal solution and that no formation of solids from the liquid mixture occurs. Aqueous phase partitioning parameters and aqueous phase reactions are adopted from the MECCA chemistry module (Sander et al., 2011).

2.1.3 Treatment of the aqueous phase in model runs

The model reads LWC (in units m^3/m^3) from the input each hour of the simulation. LWC is distributed over multiple droplets of a fixed size, 3 µm diameter, in the model runs. This means all droplets are of the same size in the simulation. Droplet diameter remains constant throughout the model runs. The number of droplets, N_d, is calculated by:

$$N_d = \frac{LWC}{\frac{4}{3}\cdot\pi\cdot r_d^{\,3}} \quad (3)$$

This approach implies that if LWC changes, the droplet number will change. Microphysics of fog or cloud formation was not considered in the model. The droplet diameter is used in MAFOR to calculate uptake rates of gases into the droplets (in terms of a forward reaction rate constant). The aqueous phase chemistry is solved for the total LWC.

To demonstrate the maximum impact of the aqueous phase of fog and cloud on tropospheric chemistry, the following example is given. Consider LWC to be 300 mg m^{-3} and that all droplets have a radius of 1 µm. Then about $7x10^4$ droplets per cubic centimeter exist, which corresponds to a maximal possible droplet number. Even then, the total air volume occupied by cloud droplets is small (10^{-7} to 10^{-6}). This means that the presence of droplets will not generate pronounced gradients in the concentration of a gas phase compound due to transfer between gas and aqueous phase and it may be assumed that gas phase compounds are well mixed within the air parcel. In this

work, with LWC of 100 mg m^{-3} and droplet radius of 3 µm, the total droplet number is about 1000 # cm^{-3}, which is certainly more realistic for fog in Norway.

In the model simulations of this work, pH is prescribed to the runs as constant value (average of rain pH measurement. In the different seasons, pH varied between from 5.1 to 5.3. Larger variation of pH values in fog or cloud was therefore not studied. In order to find out to which extent the added amine may influence the droplet pH, the pH value in the model fog using the initial chemical composition of the aqueous phase as given in Table 3 was calculated with and without the presence of amines (250 pptv in the gas phase). The resulting pH difference was only 0.23; thus it was concluded that it is reasonable to prescribe pH to the model runs.

2.1.4 Model simulation of fog cycles

The box model will consider fog cycles by distributing the given liquid water content to a monodisperse fog droplet distribution as described in section 1.2.3. Note that the simplified assumption of a monodisperse drop distributions – as compared to a more realistic polydisperse distribution – will not affect our results since thermodynamic equilibrium between gas and aqueous phase will be assumed in order to derive an upper limit estimate of the effects of chemical aqueous phase processes. While this model approach is limited in its microphysical abilities, i.e. fog formation as a function of ambient aerosol particles, it has been proven to be sufficient in order to explain gas/aqueous phase partitioning and processing of amines and nitrosamines (Hutchings et al., 2010). Fog cycles of a monodisperse fog droplet distribution were simulated with the coupled multiphase model MAFOR (Karl et al., 2011b) without taking into account the aerosol dynamic processes. No uptake of gases to interstitial aerosol particles was allowed during fog events.

In model simulations with repeated fog cycles the following treatment of aqueous phase compounds was made. With the beginning of a fog event, compounds of the gas phase were allowed to partition to the fog droplets according to their effective Henry's law coefficient. After fog dissipation, 1) dissolved neutral compounds were evaporated so that the material was transferred back into the gas phase and 2) dissolved ionic compound remained on the dry particles; in the next fog event the material was diluted so that the aqueous phase concentrations present at the end of the previous fog event were restored.

Amine salts have sufficiently low vapour pressures to partition to the aerosol phase (Angelino et al., 2001; Mäkelä et al., 2001; Murphy et al., 2007; Salo et al., 2011; Karl et al., 2012), and therefore the assumption that the amines remain in the (dry) particle phase after fog dissipation is justified; however in reality a certain fraction of the amine mass in the aqueous phase will evaporate together with water, and this was not taken into account by the model.

2.1.5 Mass balance considerations

Mass balance between the gas phase and the aqueous phase was inspected in model runs with an initial concentration of 250 pptv (i.e. 6.50 molecules cm^{-3}) dimethylamine (DMA) in the gas phase, without amine emissions. DMA levels were chosen to be representative for concentrations in a plume from an industrial or agricultural point source. The first hour of the simulation was gas phase only and after this one or several fog events with a constant LWC of 100 mg m^{-3} followed. The overall mass balance was closed and in all cases the relative error due to numerical mass loss is now less than 0.05%.

Figure 5 shows DMA concentrations in the gas phase and aqueous phase, 1) for a model run with chemical loss of DMA by OH-reaction in the gas phase (black solid line) and aqueous phase (orange dash-dotted line) and 2) for a model run without chemical loss of DMA (green and yellow dash-dotted lines). In the latter run the mass balance can be inspected. Due to mass conservation it is required:

$$[DMA]_{tot} = [DMA(t=0)] \equiv [DMA]_g + [DMA]_{aq} \quad (4)$$

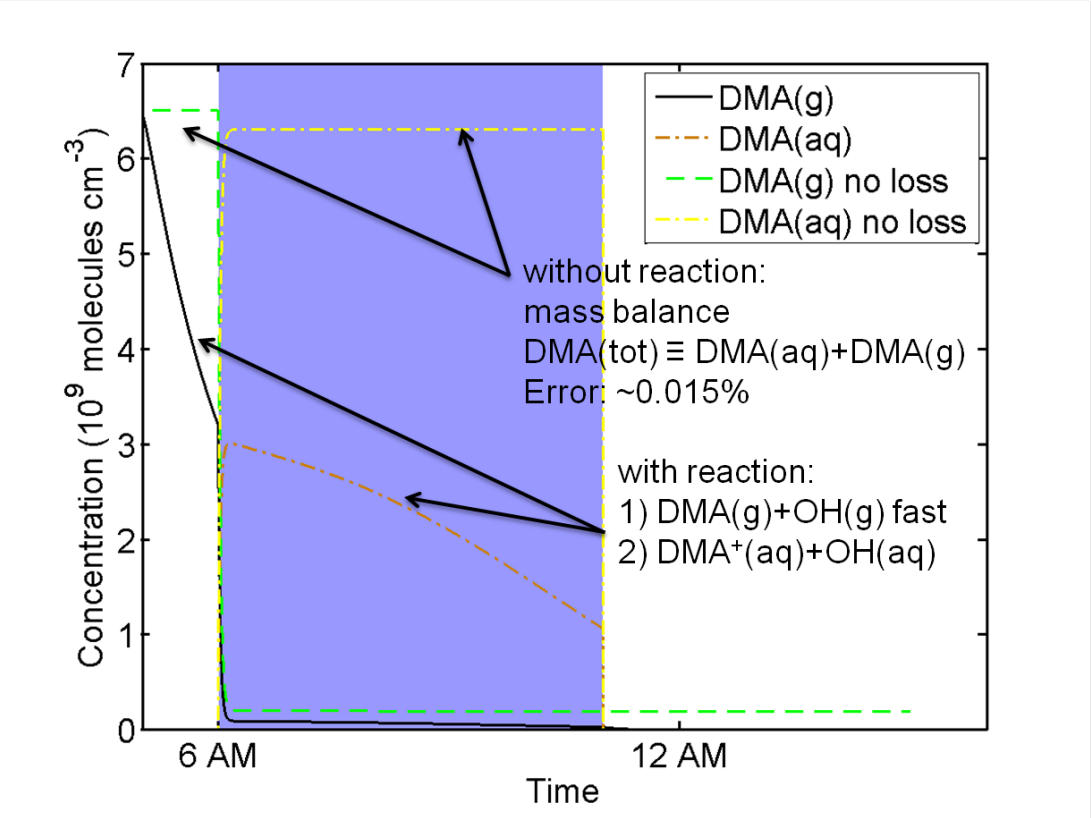

Figure 5: Test of mass conservation for DMA. Model run with chemical loss of DMA by OH-reaction in the gas phase (black solid line) and aqueous phase (orange dash-dotted line) and model run without chemical loss of DMA (green and yellow dash-dotted lines).

In the first model run, gas phase DMA (black solid line) is depleted by reaction with OH to about the half of the initial concentration. Only a small fraction remains in the gas phase when the fog starts at 6 p.m.. The major fraction partitions into the aqueous phase of the fog and the aqueous phase DMA is depleted during the fog period by reaction with OH_{aq}.

In the second model run, gas phase DMA (dash-dotted green line) remains at the level of the initial concentration until the fog starts. Only 3% of the initial DMA resides in the gas phase while 97% partition to the aqueous phase. The DMA level in the aqueous phase remains constant. The numerical error of the mass balance is only about 0.015% in this test.

In order to check the reliability of the mass conservation between gas-phase and aqueous phase a test with multiple fog events was studied. Each fog event lasted for 1 hour, at constant LWC of 100 mg m^{-3}.

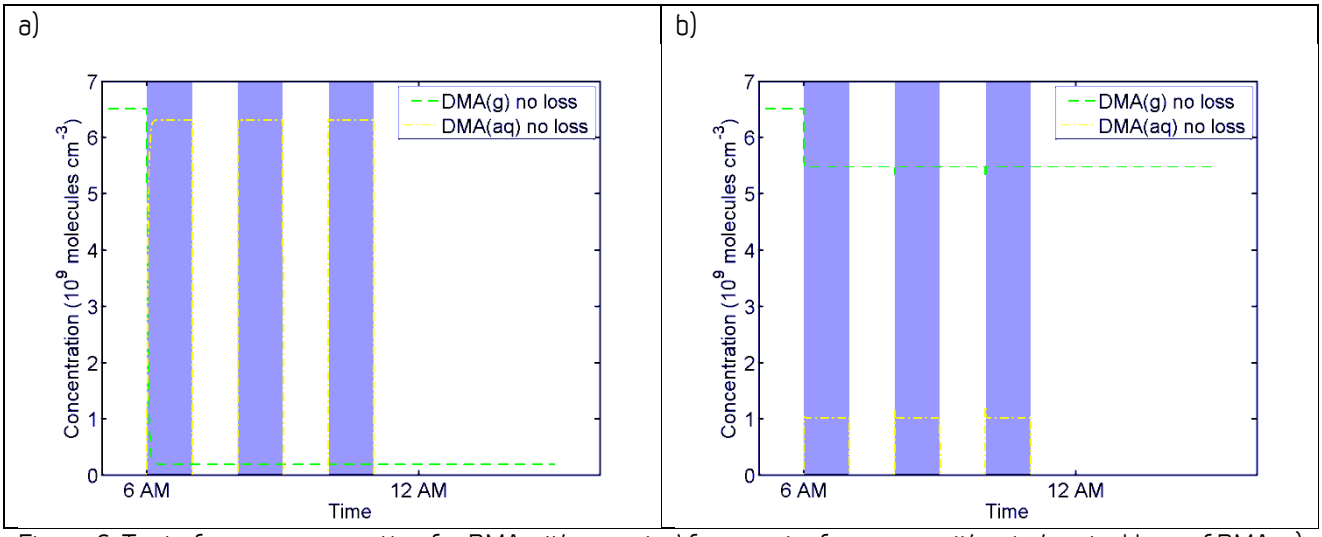

Figure 6: Test of mass conservation for DMA with repeated fog events, from runs without chemical loss of DMA: a) using the original pK_a of DMA, i.e. pK_a = 10.73, b) using pK_a = 8.5. Gas phase DMA concentrations are shown with green dash-dotted line and aqueous phase concentrations of DMA are shown with yellow dash-dotted line.

Figure 6 a) shows that mass conservation also holds for repeated fog events. No changes occur after the first fog is over because gas phase and aqueous phase are equilibrated.

At this point, it is noted that the model implements the acid-base dissociation equilibrium with the kinetics of a forward and backward reaction:

$(CH_3)_2NH_2^+(aq) \rightarrow (CH_3)_2NH(aq) + H^+(aq)$ $\quad k_f = 3.5\text{x}10^{-4}\ s^{-1}$

$(CH_3)_2NH(aq) + H^+(aq) \rightarrow (CH_3)_2NH_2^+(aq)$ $\quad k_b = 1.88\text{x}10^{7}\ M^{-1}\ s^{-1}$

where $K_a = k_f/k_b$. (5)

In a further test, the pK_a of DMA was changed to 8.5, in order to obtain a larger fraction of DMA in the gas phase during fogs. To this end, *kf* was changed to $5.9\text{x}10^{-2}\ s^{-1}$, while the same k_b was used. As shown in Figure 6 b), the fraction of DMA that remains in the gas phase is roughly 85% at pKa = 8.5. Uptake into the aqueous phase is faster at pK_a = 8.5 ($K_a = 3.16\text{x}10^{-9}$), as expected since equilibration time is proportional to the Henry's Law constant. A lower pK_a translates into a smaller effective Henry's Law constant, i.e. $K_H^{eff} = 31^*(1+1\text{x}10^{-5}/3.16\text{x}10^{-9}) = 9.8\text{x}10^4$ M atm^{-1} compared to $1\text{x}10^7$ M atm^{-1} with the original pK_a.

The small peak at the beginning of the second and third fog event illustrate that the short equilibration time poses a challenge to the solver. However, the computed aqueous phase concentration at each time step is in accordance with the mass balance. The observed behavior of the model's mass balance in all tests is indicative for a mere (and very small) numerical error of the solver and no systematic deviations from the mass closure were found.

Since DMA in the aqueous phase is almost entirely in the protonated form (dimethyl aminium, DMA^+), DMA is not transferred back to the gas phase after fog dissipation. The mass is not lost from the system because the model keeps tracking it. The DMA mass is transferred into dry particulate matter after fog dissipation and it is added to the droplets when the next fog cycle begins. Therefore the aqueous phase concentration of the next fog cycle starts with a value greater than zero. Since in reality a certain fraction of the amine may evaporate together with

the water and during the following dry period, the aqueous phase concentration at the beginning of the next fog cycle is an upper value, assuming that indeed all is converted into particulate salts. However, the procedure assures that all mass of the aqueous phase is preserved.

In the model runs, particulate mass concentrations of aminium (DMA^+) after fog dissipation were 0.23 µg m^{-3}. For comparison, Sorooshian et al. (2008) reported on levels of up to 0.18 µg m^{-3} diethylamine (corresponding to 6% of the particulate organic mass) in the plume of a feedlot. Average and maximum particulate amine concentrations measured on a flight through the plume were found to be 0.23 µg m^{-3} and 0.86 µg m^{-3} in terms of the molecular weight of methylamine, respectively. Thus the assumption of complete transfer of the amines from the droplets into the dry particles after fog dissipation (or cloud evaporation) appears to be realistic.

2.2 Gas phase mechanism of amines

The detailed reaction mechanisms of MMA, DMA, TMA, MEA, DEA, and TEA in the gas phase used in the modelling of this work are presented in Table 1 ("Gas phase reactions") of the Report Supplement "The Chemical Mechanism of MAFOR v1.4". The gas phase chemistry mechanism for amines used in this work comprises in total 70 compounds, 67 thermal reactions and 5 photolysis reactions.

2.2.1 Methylamine

A chemical scheme for the OH-initiated oxidation of methylamine (MMA) has been developed in the ADA project "Atmospheric Degradation of Amines - Photo-oxidation of Methylamine, Dimethylamine and Trimethylamine" (Nielsen et al., 2011a). Based on the results from on-line and in situ instrumentation it was found that around 25 % of the reaction between methylamine and OH radicals takes place at the amino group ($-NH_2$), and that the nitramine of MMA, methylnitramine (CH_3NHNO_2) is formed directly as a result of this (Nielsen et al., 2011a). For rural regions with NO_x levels of 0.2-10 ppbv and with a NO_2:NO ratio of 2:1, it was estimated that the yield of methylnitramine is less than 0.4 % (Nielsen et al., 2011a). The updated reaction scheme for MMA, as validated with chamber experiments in the EUPHORE reactor is presented in Figure 7.

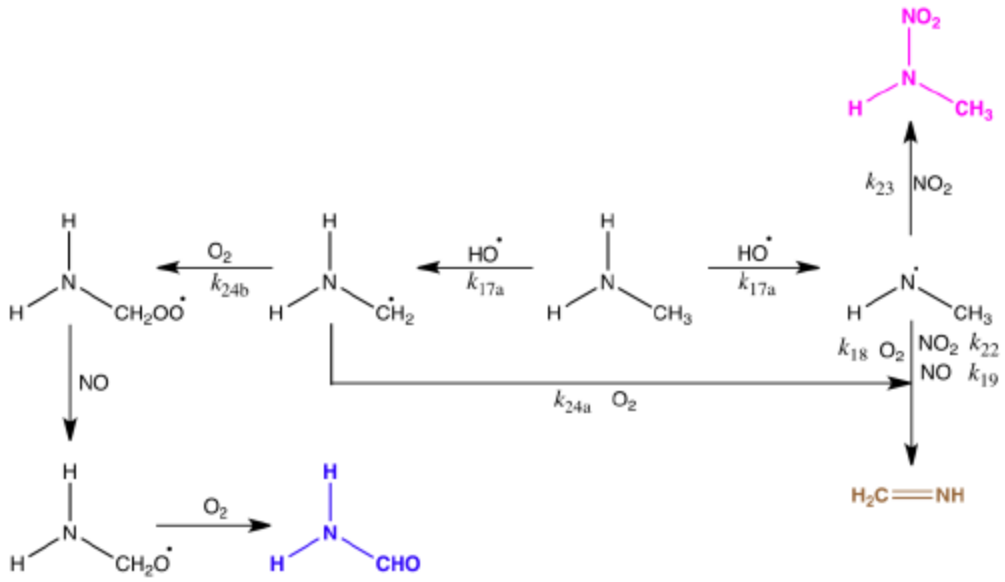

Figure 7: Reaction scheme for the photo-oxidation of methylamine with OH radicals. Adopted from Nielsen et al. (2011a).

It is noted that no nitrosamine formation was detected in the photo-oxidation of MMA. The chemical scheme for MMA used in this work is based on the updated ADA mechanism.

2.2.2 Dimethylamine

A chemical scheme for the OH-initiated oxidation of dimethylamine has been developed in the ADA project "Atmospheric Degradation of Amines - Photo-oxidation of Methylamine, Dimethylamine and Trimethylamine" (Nielsen et al., 2011a). The results from the ADA project confirmed the earlier results on nitrosamine and nitroamine formation in the OH-initiated oxidation of DMA by Lindley et al. (1979). Nielsen et al. (2011a) reported

that around 40 % of the reaction with OH radicals takes place at the amino group (–NH), and that the nitrosamine of DMA, N-nitroso dimethylamine (NDMA, $(CH_3)_2NNO$), and the nitramine of DMA, dimethylnitramine (DMN, $(CH_3)_2NNO_2$), are formed as a result of this.

For rural regions with NO_x levels of 0.2-10 ppbv and with a NO_2:NO ratio of 2:1, it was estimated that the yield of dimethylnitramine is less than 2.5 % (Nielsen et al., 2011a). The amount of NDMA forming in the atmosphere depends not only on the ambient amounts of NO and NO_2, but also on the amount of oxidizing radicals and the actinic flux. For conditions representative for the annual average of actinic flux and radical concentrations at Mongstad the calculated steady-state nitrosamine concentration was less than 0.6 % of photo-oxidized dimethylamine and less than 1.1 % of photo-oxidized trimethylamine (Nielsen et al., 2011a).

The updated reaction scheme for DMA, as validated with chamber experiments in the EUPHORE reactor is presented in Figure 8.

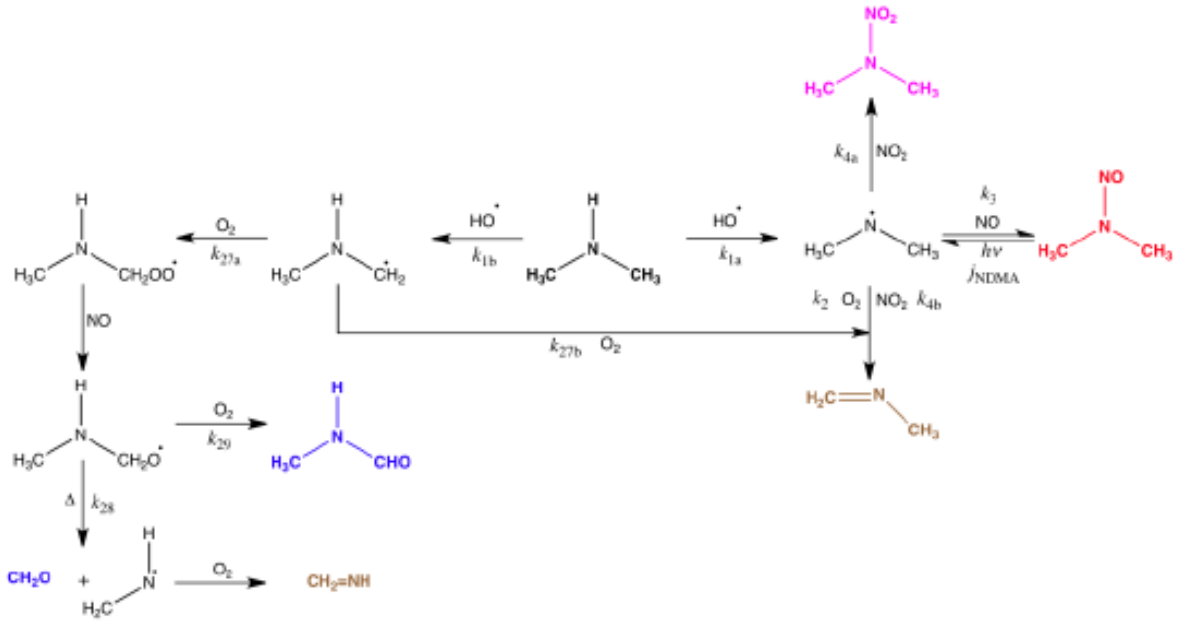

Figure 8: Reaction scheme for the photo-oxidation of dimethylamine with OH radicals. Adopted from Nielsen et al. (2011a).

The chemical scheme for DMA used in this work is based on the updated ADA mechanism.

2.2.3 Trimethylamine

A chemical scheme for the OH-initiated oxidation of trimethylamine (TMA) has been developed in the ADA project "Atmospheric Degradation of Amines - Photo-oxidation of Methylamine, Dimethylamine and Trimethylamine" (Nielsen et al., 2011a). The results from the ADA project showed that around 60 % of the reaction of TMA with OH radicals has the potential to form NDMA and DMN. For rural regions with NO_x levels of 0.2-10 ppbv and with a NO_2:NO ratio of 2:1, it was estimated that the yield of dimethylnitramine is less than 5 % (Nielsen et al., 2011a).

The updated reaction scheme for TMA, as validated with chamber experiments in the EUPHORE reactor is presented in Figure 9.

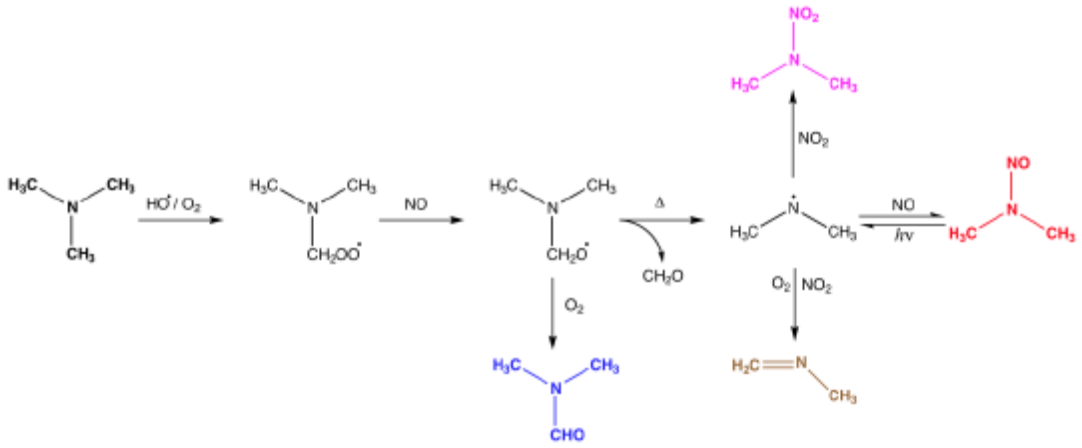

Figure 9: Reaction scheme for the photo-oxidation of trimethylamine with OH radicals. Adopted from Nielsen et al. (2011a).

The chemical scheme for TMA used in this work is based on the updated ADA mechanism.

2.2.4 Monoethanolamine

The chemical scheme for the OH-initiated oxidation of 2-aminoethanol (monoethanolamine, MEA) used in this work (Karl et al., 2012) has originally been constructed during the project ADA-2009 ("Atmospheric Degradation of Amines - Gas phase photo-oxidation of 2-aminoethanol (MEA)" by Nielsen et al. (2010), based on quantum chemical calculations (Bråten et al., 2008), structure activity relationship (SAR) estimated rate constants and adjusted to fit experimental data in MEA photo-oxidation experiments in EUPHORE. The scheme contains 17 reactions and 17 compounds in the gas phase.

According to Nielsen et al. (2011b), the formation of the following products was unambiguously attributed to the OH-initiated oxidation of MEA in the EUPHORE experiments: formaldehyde (HCHO), formamide (H_2NCHO), amino acetaldehyde (H_2NCH_2CHO), 2-oxo-acetamide ($H_2NC(O)CHO$), 2-imino ethanol ($HN{=}CHCH_2OH$) and the 2-nitroamino ethanol (for more details it is referred to Table 1 in the publication by Nielsen et al., 2011b). Average branching ratios of the initial H-abstraction given by Nielsen et al. (2011b) are 8% from $-NH_2$, 84% from $-CH_2-$ and 8% from $-CH_2OH$. Karl et al. (2012) gave slightly modified branching ratios: 15 %, 80 %, and 5% for the $-NH_2$, $-CH_2-$, and $-CH_2OH$ positions, respectively.

The nitrosamine of MEA; 2-nitroso amino ethanol, was not detected by Karl et al. (2012) in the experiments with any of the methods, in line with the findings by Nielsen et al. (2011b). The published reaction mechanism by Karl et al. (2012) still includes the formation of the nitrosamine with a very small yield and its rapid destruction by photolysis. Theoretical studies (Angove et al., 2010) suggest that 2-nitroso amino ethanol partly undergoes immediate isomerisation to 2-hydroxydiazenyl ethanol ($HOCH_2CH_2N{=}NOH$) which then decomposes to give 2-imino ethanol.

The product yield of the nitramine of MEA, 2-nitroamino ethanol in different experiments in EUPHORE under various NO_x levels were reported to range between 0.3% and 1.5% (Nielsen et al., 2011b). Comparison of modelled and measured concentrations of 2-nitroamino ethanol indicate that the model currently overestimates the production yield of the nitramine by at least a factor of 5 (Karl et al., 2012).

2.2.5 Diethanolamine

The OH-initiated oxidation of diethanolamine (DEA), a secondary alkanolamine, in the gas phase has not been studied in detail until now. Therefore it was decided to derive a chemical scheme based on analogies to DMA. The branching ratios of the initial H-abstraction was taken to be identical with the branching ratios of DMA. Therefore the photo-oxidation of DEA was postulated to form the nitramine, diethanolnitramine (DEN), and the nitrosamine, N-nitroso diethanolamine (NDELA) with the same yields as DMA. This treatment probably overestimates the formation potential of DEA, because the molecule contains weaker secondary C–H bonds than DMA. However, the expected faster rate of H-atom abstraction form the ethanol groups in DEA compared to that from the methyl groups in DMA might be accompanied by a correspondingly faster rate of H-atom abstraction from the N–H bond, as has been suggested by Tuazon et al. (2011) for the diethylamine.

In addition certain steps of the reaction mechanism of DEA and TEA were tentatively based on the chemical scheme presented for N-methyl diethanolamine (MDEA) by Bråthen et al. (2008). Figure 10 shows the main routes of the predicted photo-oxidation scheme of MDEA following initial hydrogen abstraction from one of the ethanol groups.

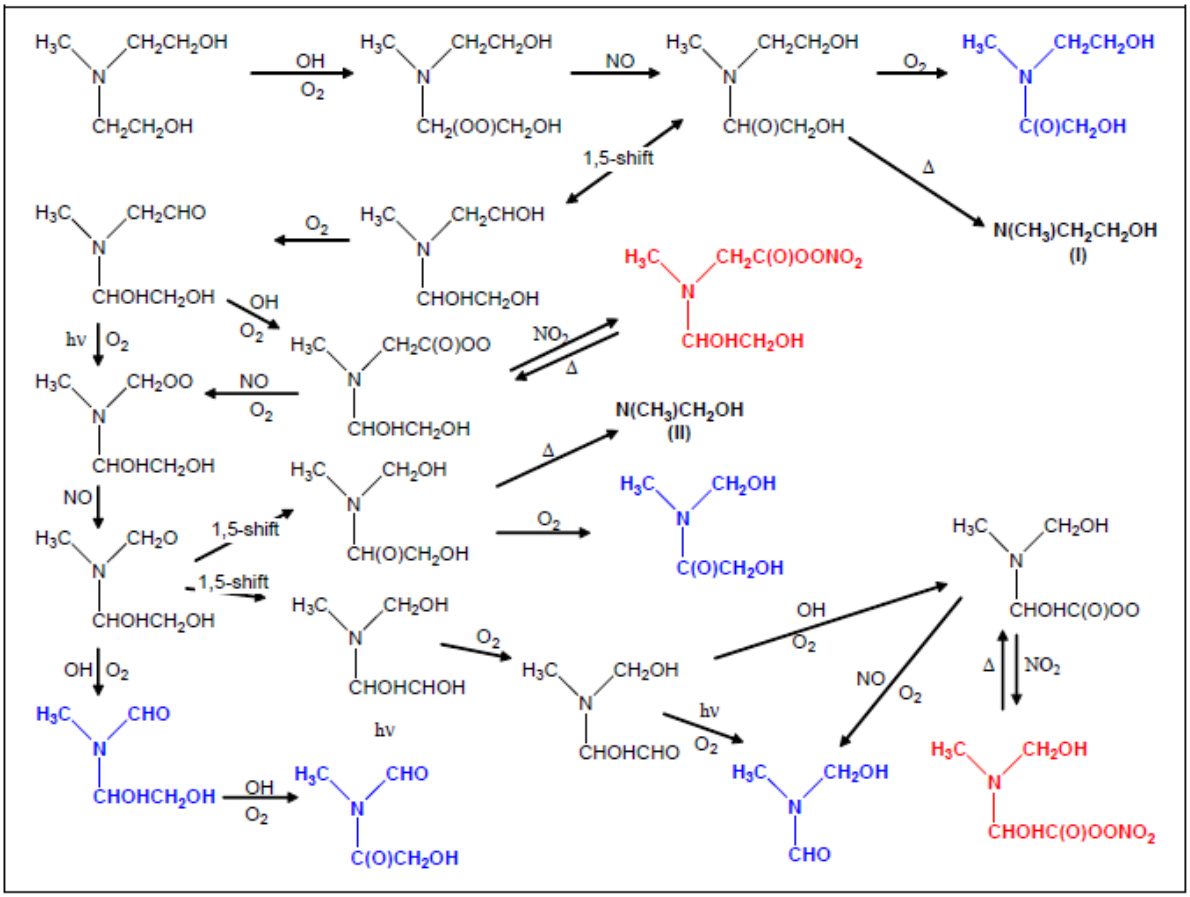

Figure 10: Reaction scheme for the photo-oxidation of MDEA with OH radicals following initial hydrogen abstraction from one of the ethanol groups. Adopted from Bråthen et al. (2008).

Since the focus of this work is on the aqueous phase production of nitrosamines and nitroamines, the validity of the postulated DEA mechanism might be less crucial.

2.2.6 Triethanolamine

The OH-initiated oxidation of triethanolamine (TEA), a tertiary alkanolamine, in the gas phase has not been studied in detail until now. Therefore it was decided to derive a chemical scheme based on analogies to TMA. The reaction sequence following initial hydrogen abstraction from one of the ethanol groups was based on the theoretical scheme for MDEA by Bråthen et al. (2008), see Figure 10.

2.3 Aqueous phase mechanism of amines

The detailed reaction mechanisms of MMA, DMA, TMA, MEA, DEA, and TEA in the aqueous phase used in the modelling of this work are presented in Table 8 ("Aqueous phase reactions") of the Report Supplement "The Chemical Mechanism of MAFOR v1.4". The aqueous phase chemistry mechanism for amines used in this work comprises in total 69 compounds, 58 irreversible aqueous phase reactions, 36 Henry's law partitioning equilibria, 38 dissociation (acid-base) equilibria and 7 photolysis reactions. Table 3 ("Henry's law coefficients") in the Supplement provides the Henry's law constants of all partitioning compounds and Table 4 ("Accommodation coefficients") provides the accommodation coefficients of all compounds that are taken up into the aqueous phase.

Reactions related to the aqueous phase production of nitrosamines and nitroamines are treated in detail in section 1.6.

2.3.1 Methylamines

Of the amines under investigation, the OH-initiated oxidation of TMA in the aqueous phase has been studied most thoroughly (Das and von Sonntag, 1986; Das et al.; 1987). Main products in basic solution are dimethylamine, formaldehyde and hydrogen peroxide (Das et al., 1987). In competition to the abstraction of a carbon bound hydrogen atom, abstraction of the nitrogen-bound hydrogen atom may also occur, producing the radical cation. For TMA, three different radicals form after H-abstraction by OH (Das and von Sonntag, 1986): the N-centred radical cation ($(CH_3)_3N^{+\bullet}$), the C-centred radical ($(CH_3)_2NCH_2^{\bullet}$), and the protonated C-centred radical ($(CH3)_2HN^{+}CH_2^{\bullet}$. Hydroxyl radicals react in general about two orders of magnitudes faster with the unprotonated alkyl amine than with the protonated form (aminium). Das and von Sonntag (1986) provided a detailed chemistry mechanism for OH-oxidation of TMA including rate constants derived from best fit to experiments. This mechanism forms the basis for the reaction scheme of TMA developed in this work. The reaction schemes for the OH-initiated oxidation of MMA and DMA in the aqueous phase follow analogous considerations.

2.3.2 Ethanolamines

Some aspects of the OH-initiated oxidation of the ethanolamines MEA, DEA and TEA were investigated by Kishore et al. (2004). Due to the remaining knowledge gaps, the aqueous phase mechanism for TMA by Das and von Sonntag (1986) was used as a template to set up corresponding aqueous phase mechanisms for the ethanolamines. Kishore et al. (2004) suggested that the N-centred radical cation forms in the OH-oxidation of the ethanolamines, i.e. $H_2N^{+\bullet}$–R for MEA, $HN^{+\bullet}$–R_2 for DEA and $R_3N^{+\bullet}$ for TEA, where R = –CH_2CH_2OH. Formaldehyde and the amino methyl radical ($^{\bullet}CH_2NH_2$) are probably the main products of the oxidation of MEA with OH in the aqueous phase.

2.4 Partitioning and acid-base equilibria

Phase transfer processes are important considerations for the formation and photolysis of nitrosamines and nitramines. Formation/destruction mechanisms and kinetics will depend on the phase the reactive species are in. In many instances it is a valid approach to assume equilibrium between phases. At the current state of understanding, too little data is available to investigate if mass transfer limitations will impact overall formation and destruction rates. No information exists on mass accommodation coefficients for the species under investigation.

2.4.1 Partitioning of amines, amides, nitrosoamines and nitroamines

Table 4 provides an overview of the Henry's law constants and accommodation coefficients for methylamines, ethanolamines and their possible oxidation products.

Table 4: Henry's law constants and accommodation coefficients of amines, amides, nitrosamines and nitramines used in the model. No temperature dependence of the Henry's coefficients and the accommodation coefficients was assumed.

Compound	Henry's constant (@298.15 K) mol kg^{-1} atm^{-1}	Accommodation coefficient	Reference Henry's constant
Monomethylamine	36.5	0.1	Ge et al. (2011)
Dimethylamine	31.4	0.1	Ge et al. (2011)
Trimethylamine	9.6	0.1	Ge et al. (2011)
Monoethanolamine	6.18×10^{6}	0.1	Ge et al. (2011)
Diethanolamine	2.58×10^{7}	0.1	Ge et al. (2011)
Triethanolamine	1.42×10^{9}	0.1	Ge et al. (2011)
Methylnitramine	685	0.1	EPIWin4.1 Bond method
Dimethylnitramine	313	0.1	EPIWin4.1 Bond method
MEA-nitramine	4.45×10^{6}	0.1	SM8 calculated
DEA-nitramine	2.37×10^{9}	0.1	SM8 calculated
N-nitroso dimethylamine	275	0.1	EPIWin4.1 Bond method
N-nitroso ethanolamine	2.06×10^{8}	0.1	EPIWin4.1 Bond method
N-nitroso diethanolamine	1.00×10^{7}	0.1	EPIWin4.1 Bond method
Isocyanic acid	25.0	0.1	Roberts et al. (2011)
Formamide	7.19×10^{5}	0.1	Ge et al. (2011)
2-Hydroxy acetamide	5.83×10^{5}	0.1	Ge et al. (2011)
N-Methyl formamide	2.98×10^{4}	0.1	EPIWin4.1 Bond method
N,N-Dimethyl formamide	1.36×10^{4}	0.1	EPIWin4.1 Bond method

Henry's law constants of amines and amides were taken from a recent review paper by Ge et al. (2011), who provided an extensive review of known physicochemical parameters of amines. Henry's Law constants for methylamine, dimethylamine and trimethylamine are reported to be 39 - 90 mol kg^{-1} atm^{-1}, 31 - 57 mol kg^{-1} atm^{-1}, and 9.6 mol kg^{-1} atm^{-1}, respectively (Wilhelm et al., 1977; Christie and Crisp, 1967). Henry's Law constants for

monoethanolamine (MEA), diethanolamine (DEA) and triethanolamine (TEA) are estimated to be $6.18x10^6$, $2.58x10^7$ and $1.42x10^9$ mol kg^{-1} atm^{-1}, respectively (Ge et al., 2011). The K_H value of MEA is based on laboratory data reported by Bone et al. (1983).

For the partitioning of nitrosamines, nitroamines and several amides no experimental data was available. For these compounds, the Henry's law coefficients were estimated with the U.S. EPA Software EPI Win4.1 using the bond contribution method. The bond contribution method estimates the Henry's Law constant of organic compounds at 25°C using the methodology originally described by Hine and Mookerjee (1975). The original bond contribution methodology was updated and expanded in EPI Win4.1 as described in Meylan and Howard (2000).

In an alternative approach, Henry's law constants have been calculated with the SM8 solvation model (Marenich et al., 2007) as it is implemented in the Spartan 08 code. This is a continuum solvation model, utilized in combination with a quantum mechanical representation of the solute. The calculations were carried out at the SM8-M06/6-31+G*level of theory, with the solute geometry optimized with the continuum solvation model. Calculations were carried out for the most stable conformer found for each solute. The model calculates solvation free energies and these are then converted to Henry's law constants. The uncertainty in the calculations is expected to be in around +/-0.5 kcal/mol in solvation energies. ***Table 5*** summarizes the Henry's law constants as computed with the SM8 solvation model.

Table 5: Henry's law constants and solvation energies as computed with solvation model SM8.

	Henry's constant (@298.15 K) mol kg^{-1} atm^{-1}	**dG(Solvation) SM8 kcal mol^{-1}**	**Compound**	**Henry's constant (@298.15 K) mol kg^{-1} atm^{-1}**	**dG(Solvation) SM8 kcal mol^{-1}**
Monomethylamine	84.6	-8.0	DEA-nitramine	$2.37x10^9$	-114.7
Dimethylamine	50.5	-4.2	N-nitroso dimethylamine	863	-5.9
Trimethylamine	16.2	-3.5	N-nitroso ethanolamine	$6.36x10^5$	-9.8
Monoethanolamine	$4.52x10^4$	-8.2	N-nitroso diethanolamine	$1.45x10^8$	-13.0
Diethanolamine	$1.26x10^6$	-10.2	Isocyanic acid	12.8	-3.4
Triethanolamine	$3.05x10^4$	-4.5	Formamide	$3.67x10^6$	-10.8
Methylnitramine	$4.78x10^4$	-8.3	2-Hydroxy acetamide	$1.10x10^8$	-12.8
Dimethylnitramine	$1.99x10^4$	-7.7	N-Methyl formamide	$3.03x10^4$	-8.0
MEA-nitramine	$4.45x10^6$	-10.9	N,N-Dimethyl formamide	$1.85x10^3$	-6.3

2.4.2 Acid-base equilibria of amines

The acidity constants for the acid-base dissociation equilibria, K_a and pK_a, of compounds used in the modelling in this work are summarized in.

Table 6: Acid-base equilibria of amines and amides: pKa values used in the model.

Compound	pKa	Ka mol kg^{-1}	Reference pKa
Monomethylamine	10.66	$2.19x10^{-11}$	Ge et al. (2011)
Dimethylamine	10.73	$1.86x10^{-11}$	Ge et al. (2011)
Trimethylamine	9.76	$1.74x10^{-10}$	Ge et al. (2011)
Monoethanolamine	9.40	$3.98x10^{-10}$	Kishore et al. (2004)
Diethanolamine	8.93	$1.17x10^{-9}$	Kishore et al. (2004)
Triethanolamine	7.78	$1.66x10^{-8}$	Kishore et al. (2004)
Isocyanic acid	3.70	$2.00x10^{-4}$	Roberts et al. (2011)

2.4.3 Effective Henry's law constants of amines

The partitioning of amines between the gas and aqueous phases inside fog or cloud is defined by the effective Henry's law constant, which depends on the droplet's pH. Effective Henry's law constants for the amines investigated in this work are provided in Table 7 for different pH values between 1 and 9. More data on effective Henry's law constants of amines and amides is presented in the report of WP1 ("D1 - Evaluation of the Atmospheric Chemistry Status overview").

Table 7: Effective Henry's law constants of amines, calculated for pH=1 to pH=9, at 298. 15K.

Amine	K_H^{eff} (in mol kg^{-1} atm^{-1}), for pH 1 to 9				
	9	7	5	3	1
Monomethylamine	1.7038E+03	1.6677E+05	1.6673E+07	1.6673E+09	1.6673E+11
Dimethylamine	1.7182E+03	1.6871E+05	1.6868E+07	1.6868E+09	1.6868E+11
Trimethylamine	7.0361E+01	6.0832E+03	6.0736E+05	6.0735E+07	6.0735E+09
Monoethanolamine	4.1742E+07	3.5624E+09	3.5563E+11	3.5562E+13	3.5562E+15
Diethanolamine	5.1052E+07	2.5490E+09	2.5235E+11	2.5232E+13	2.5232E+15
Triethanolamine	1.4985E+09	9.5710E+09	8.1682E+11	8.1541E+13	8.1540E+15

Dissociation of amines in aqueous solution can be written as:

$R_nNH_{4-n}^+(aq) \quad \Leftrightarrow \quad R_nNH_{3-n}(aq) \quad + \quad H^+(aq)$ (I)

Where n=1, 2, or 3 signifies primary, secondary or tertiary amine.

The dissociation equilibrium constant K_a is then expressed as:

$$K_a = \frac{\left(\left[R_nNH_{3-n}\right]\left[H^+\right]\right)}{\left[R_nNH_{4-n}^+\right]} \quad (2)$$

The total amine concentration in the aqueous phase is the sum of the unprotonated amine and the protonated amine (=aminium). The effective Henry's law constant K_H^{eff} is defined as:

$$K_H^{eff} = \frac{\left(\left[R_nNH_{3-n}\right]_{aq} + \left[R_nNH_{4-n}^+\right]_{aq}\right)}{\left[R_nNH_{3-n}\right]_g} \quad (3)$$

Solving Eq. (2) for $[R_nNH_{4-n}^+]_{aq}$ and substituting in Eq. (3), and splitting into two additive terms with the same denominator gives:

$$K_H^{eff} = \frac{\left[R_nNH_{3-n}\right]_{aq}}{\left[R_nNH_{3-n}\right]_g} + \frac{\left[R_nNH_{3-n}\right]_{aq} \cdot \left[H^+\right]_{aq}}{\left[R_nNH_{3-n}\right]_g} \quad (4)$$

By replacing $[R_nNH_{3-n}]_{aq}/[R_nNH_{3-n}]_g$ with the Henry's law constant K_H (physical solubility) a simple expression for the effective Henry's law constant is derived:

$$K_H^{eff} = K_H + K_H \frac{\left[H^+\right]}{K_a} = K_H \cdot \left(1 + \frac{\left[H^+\right]}{K_a}\right) \quad (5)$$

As an example, for pH = 5, the effective Henry's law constant of dimethylamine is:

K_H^{eff} = 31.4 mol kg^{-1} atm^{-1}*(1 + (1x10^{-5}mol kg^{-1}/1.86x10^{-11} mol kg^{-1})) ≈ 1.7x10^7 M atm^{-1}.

The fraction of the unprotonated amine to the total dissolved amine concentration can be calculated simply by:

$$\frac{\left(\left[R_nNH_{3-n}\right]_{aq}\right)}{\left(\left[R_nNH_{3-n}\right]_{aq} + \left[R_nNH_{4-n}^+\right]_{aq}\right)} = \frac{1}{1+10^{pKa-pH}} \quad (6)$$

For dimethylamine, the fraction of unprotonated amine to total amine is only ≈2x10^{-6} at pH = 5.

Figure 11 shows the fraction of the amine (or any other compound) that is dissolved in the aqueous phase at LWC of 100 mg m^{-3} as function of the (effective) Henry's law constant. The plot was obtained by first converting the

Henry's law constant at a given LWC (here in $L_{H2O}^{-1}/cm^3(g)$) into a dimensionless value [molecules(aq)/molecules(g)], i.e.

$K_H(\text{dimless}) = K_H[\text{mol}/ L_{H2O}^{-1}/\text{atm}] * \text{LWC} [L_{H2O}^{-1}/ \text{cm3(g)}] * N_A/[M]$ (7)

With N_A being the Avogadro's constant (N_A = 6.022x10^{23} molec mol^{-1}) and [M] being concentration of air molecules at room temperature (M = 2.5x10^{19} molec cm^{-3} atm^{-1}).

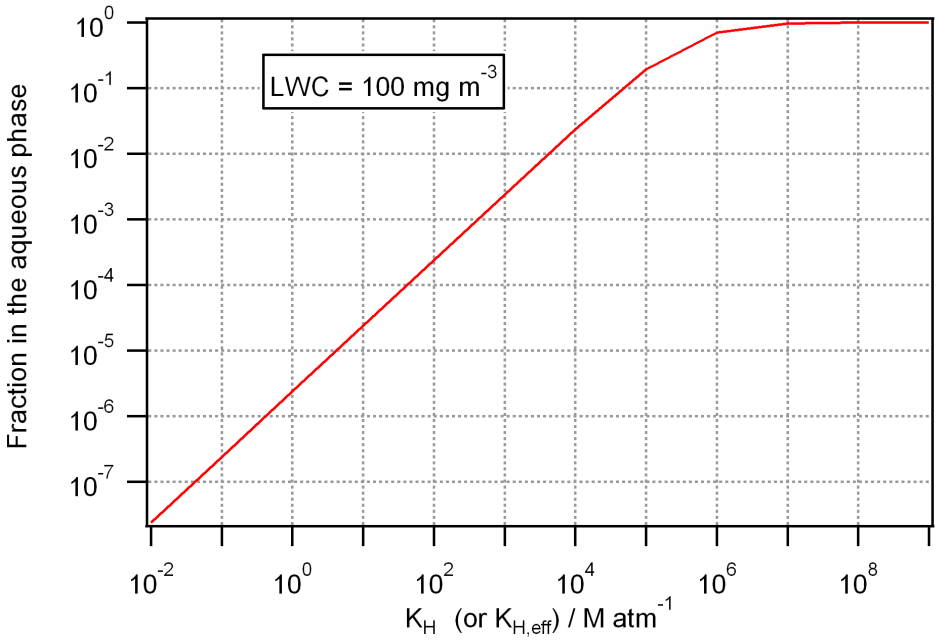

Figure 11: *Fraction of amine in the aqueous phase as function of the Henry's law constant K_H (or K_H^{eff}) at LWC of 100 mg m^{-3}. With friendly permission by B. Ervens (NOAA).*

The fraction in the aqueous phase, F_{aq}, can be derived from the dimensionless Henry's law constant by:

$$F_{aq} = \frac{K_H(\text{dimless})}{1 + K_H(\text{dimless})} \quad (8)$$

For the above example of DMA at pH=5, the KH was calculated to be 1.7x10^7 M atm^{-1}. Using the plot in Figure 11 it can immediately be seen that the fraction in the aqueous phase is ›90%.

2.5 Production and destruction of nitrosamines and nitroamines in the aqueous phase

The aqueous phase production and loss of the following nitrosamines and nitroamines is studied in this work:

Substance	Abbreviation
N-nitrosodimethylamine	NDMA
2-nitrosoamino ethanol	NMEA
N-nitrosodiethanolamine	NDELA
Methylnitramine	MMN
Dimethylnitramine	DMN
2-nitroamino ethanol	MEN
Diethanolnitramine	DEN

2.5.1 Nitrosation as third order reaction system

The best known reagent for nitrosating amines is nitrite salts or nitrous acid (HONO) in aqueous acidic solutions at pH<5 (Challis and Challis, 1982). However, neither nitrite (NO_2^-) nor HONO react directly with the secondary amines (Challis and Challis, 1982); instead they are first converted to an active nitrosating compound such as nitrous anhydride (N_2O_3) or the nitrous acidium ion (H_2ONO^+). H_2ONO^+ is a powerful nitrosating agent at strongly acidic conditions (Anastasio and Chu, 2009). Since it exists only at pH<3, nitrosation by H_2ONO^+ is not relevant in cloud and fog in remote and moderately polluted regions.

For experiments carried out at optimum pH, a large fraction of the nitrite becomes converted to HONO (pKa = 3.6), and the reaction sequence for nitrosation of secondary amines is thought to be (Mirvish, 1975):

$$2\,HONO(aq) \Leftrightarrow N_2O_3(aq) + H_2O(aq) \quad (I)$$

$$R_2NH(aq) + N_2O_3(aq) \rightarrow R_2NNO(aq) + HONO(aq) \quad (II)$$

The nitrosating agent is then N_2O_3, and the reaction is second order in nitrite (or HONO). For the overall nitrosation rate, Mirvish (1975) provided two different expressions:

1) $Rate = k_1 \cdot [R_2NH] \cdot [HONO]^2$
2) $Rate = k_2 \cdot [amine][nitrite]^2$

Expression (2) considers the total amine concentration ($[R_2NH]+[R_2NH_2^+]$) and the total nitrite concentration ($[HONO]+[NO_2^-]$). It is noted that at optimum pH, for most amines of interest in CCS, the fraction of the unprotonated amine is very small. At pH = 3.4, the fraction of HONO is about the half of the total nitrite. Expression (2) should therefore only be used to give a first estimate of the nitrosation rate based on gross amounts of amine and nitrite salt, and not for implementation into a chemistry mechanism.

A critical limitation to nitrosation is that only the unprotonated amine bases are reactive towards the nitrosating agent.

According to expression (1), one may write for the formation of N-nitroso dimethylamine (NDMA) from dimethylamine (DMA):

DMA(aq) + 2 HONO(aq) → NDMA(aq) + H_2O(aq) (III)
$k_1 = 1.5x10^5\ M^{-2}\ s^{-1}$

Hutchings et al. (2010) found that the yield of NDMA in nitrosation experiments was only 1% and introduced a stoichiometric factor of 0.01 in reaction (III). Therefore the estimated nitrosation rates by Hutchings et al. (2010) are two orders of magnitude lower than those by Mirvish et al. (1975):

DMA(aq) + 2 HONO(aq) → 0.01 NDMA(aq) + H_2O(aq)
$k_1 = 1.5x10^5\ M^{-2}\ s^{-1}$

In our work the implementation of third order nitrosation is done in the form of reaction (II):

DMA(aq) + N_2O_3(aq) → NDMA(aq) + HONO(aq) (IV)
$k_{IV} = 4.29x10^7\ M^{-1}\ s^{-1}$

Mirvish (1975) claims that the second reaction is rate-limiting, such that we can assume the first reaction (reaction (I)) reached equilibrium. Using $k_{forward}$ and $k_{backward}$ by Licht et al. (1988) and Schwartz (1983), respectively, to calculate K_{eq} of the HONO/N_2O_3 equilibrium one can derive the rate constant of reaction (IV) as $k_{IV} = k_1/K_{eq}$.

A third order reaction between DMA and NO_2^- was not included in this work, because NO_2^- would first have to be converted to HONO in order to become a nitrosating agent (according to reactions (I) and (II)).

Experiments with DEA performed in this work confirmed that nitrosation is second order in nitrite: the exact order was 1.84±0.05 when monitoring NDELA concentrations and 1.59±0.07 when monitoring nitrite concentrations (1.77±0.07 if two samples with the highest nitrite concentration were excluded). The yield of NDELA from the third order reaction was found to be ca. 85 %, showing a near quantitative conversion. The reaction of TEA with N_2O_3 showed a yield of 1.4 % NDELA at 25°C, in agreement with the upper limit of 2 % at 37°C reported by Lijinsky et al. (1972). More details on the nitrosation experiments can be found in the report **"D4 - Technical report on experimental results"**.

Based on the experiments, as upper limits for the modelling, the following yield estimates were adopted for the third order nitrosation reaction system:

- Primary amine: zero yield, reaction was neglected;
- Secondary amine: 100 % yield of the secondary nitrosamine;
- Tertiary amine: 5 % yield of the secondary nitrosamine.

The rate constant k_{IV} was determined in the experiments and found to be $1.0(\pm0.1)x10^7\ M^{-1}\ s^{-1}$ for the reaction DEA+N_2O_3 and $2.9(\pm0.13)x10^5\ M^{-1}\ s^{-1}$ for the reaction TEA+N_2O_3. These values were adopted in the modelling.

2.5.2 Nitrosation as second order reaction system

In several studies, nitrosation of secondary amines by nitrite was found to occur at higher pH, e.g. at physiological pH (e.g. Casado et al., 1984), indicative of a second order reaction system. Weller et al. (2011) suggested that the kinetics of nitrosation were first order in nitrite.

There are two possibilities to explain nitrosation of secondary amines as a second order reaction with NO_2^- (or HONO). Firstly, photolysis of nitrite in aqueous solution produces NO which may react with secondary amines to

form nitrosamines. However, NO reacts very slowly and is known to be a poor nitrosating agent (Challis and Challis, 1982). Secondly, nitrite may react with the iminium ion (R_2N^+=CH) which forms in the initial attack of a secondary amine by formaldehyde or by OH radicals (Casado et al., 1984). Evidence for the effective (›90% yield) nitrosamine formation in the reaction between the (secondary) iminium ion and nitrite was found by Keefer and Roller (1973) who reacted N,N-dimethyl formaldiminium trifluoracetate with excess of silver nitrite in anhydrous acetonitrile solution.

The initial attack proceeds probably very slowly and is the rate limiting step. However, since the iminium ion is a possible intermediate in the aqueous oxidation of amines (both unprotonated and protonated form) by OH radicals, the nitrosation pathway may be relevant.

Due to the mechanistic uncertainties, a simplified approach for the treatment of nitrosation as second order reaction system was chosen:

DMA(aq) + HONO(aq) → NDMA + H_2O(aq) (V)

and

DMA(aq) + NO_2^-(aq) → NDMA + OH^-(aq) (VI)

$k_V = k_{VI} = 0.1\ M^{-1}\ s^{-1}$.

The rate constant of 0.1 $M^{-1}\ s^{-1}$ as an upper limit value for second order nitrosation was suggested by Weller et al. (2011) and is adopted in this work.

2.5.3 Nitration as third order reaction system

The reaction of secondary amines with nitrogen tetraoxide (N_2O_4) in aqueous solution is found to produce nitroamines. Nitrosating and nitration of dimethylamine by N_2O_4 follows the following scheme:

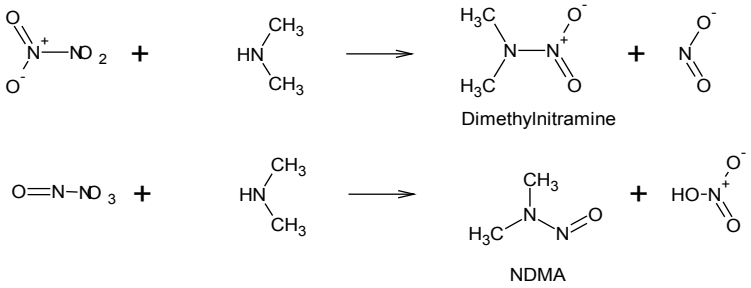

Nitrosamines are also formed in this reaction. This is because N_2O_4 exists in two tautomeric forms:

$$O{=}N{-}ONO_2 \quad \Leftrightarrow \quad O_2N{-}NO_2 \qquad \text{(VII)}$$

From these, O_2N-NO_2 is the nitrating agent while $O{=}N$-ONO_2 is a nitrosating agent.

Simple computational chemistry calculations have been carried out in order to study the relative stability of the two tautomeric forms of N_2O_4. The calculations were carried at the SM8-M06/6-31+G* level of theory. In these calculations the O_2N-N_2O form was found to be more stable by 12 kcal/mol in solution. Such an energy difference would suggest that this conformer is dominant in aqueous solution. This conclusion is consistent with results reported by Zhakarov et al. (2008).

N_2O_4 is formed in the aqueous solutions by dimerization of NO_2:

$$2\ NO_2(aq) \quad \Leftrightarrow \quad N_2O_4 \qquad \text{(VIII)}$$

N_2O_4 (in the form of O_2N-NO_2) directly reacts with the secondary amine to form the nitramine via a reaction intermediate, the protonated nitramine, which is expected to have a high energy of activation and consequently is unstable due to the repulsion between the two positively charged nitrogen atoms (Cooney et al., 1987).

Since the nitrating agent is formed from two NO_2 molecules, the overall nitration reaction of secondary amines is third order. Nitration of secondary amines is included in the model. For dimethylamine the following equation is written, assuming that 50% nitroamines and 50% nitrosamines are formed:

$$DMA(aq) + N_2O_4(aq) \rightarrow 0.5\ DMN(aq) + 0.5\ NDMA(aq) + 0.5\ HONO(aq) + 0.5\ HNO_3(aq) \qquad \text{(IX)}$$

$k_{IX} = 4.0 \times 10^7\ M^{-1}\ s^{-1}$

The rate constant for nitration, $k_{IX} = 4.0 \times 10^7\ M^{-1}\ s^{-1}$ is based on the work by Challis and Kyrtopoulos (1979). The yield of 50% nitroamines should be seen as an upper limit since observed nitramine yields for different secondary amines were typically lower.

It is noted that very high concentrations of nitrate (NO_3^-) were found to slightly enhance nitration (Cooney et al., 1987). Nitrate may react with N_2O_4 to yield nitrogen pentoxide (N_2O_5) which should be exclusively a nitrating agent. The suggested enhancement is however not relevant for concentration levels of nitrate typically observed in the atmospheric aqueous phase.

Experiments with MEA, DEA and TEA performed in this work using NO_2/N_2O_4 stock solutions revealed that N_2O_4 is likely the only nitrosating/nitrating reagent while NO_2 appears not to be reactive in the aqueous solution. Yields of nitroamines from the N_2O_4 reaction appear to be minor (<1%). Yields in the reaction of the primary amine (MEA) were negligible. NDELA was the predominant product in the experiments with DEA, with a yield of ca. 32%. The yield of NDELA in the TEA + N_2O_4 experiment was ca. 1%. More details on the nitration experiments can be found in the report "D4 - Technical report on experimental results".

Based on the experiments, as upper limits for the modelling, the following yield estimates were adopted for the third order nitration reaction system:

- Primary amine: zero yield of the nitrosamine (R_2-NNO, R = CH_3 or CH_2CH_2OH) and 30 % yield of the corresponding nitramine (based on the upper limit for aniline reported by Challis and Kyrtopoulos, 1979);
- Secondary amine: 40 % yield of the nitrosamine (R_2-NNO) and 40 % of the nitramine;
- Tertiary amine: 5 % yield of the nitrosamine (R_2-NNO) and 5 % yield of the nitramine (R_2-NNO_2).

The rate constant for nitration, k_{IX} = 4.0×10^7 M^{-1} s^{-1} is an upper limit given by Challis and Kyrtopoulos (1979) and this value was adopted for modelling.

2.5.4 Nitration as second order reaction system

A reaction mechanism between NO_2 and secondary amines to form nitroamines following second order can be justified as follows. It was suggested that hydrogen abstraction form the amine is the rate limiting step in the nitration (Cooney et al., 1987). In analogy to the gas phase reaction of NO_2 with alkenes (Giamalva et al., 1987), NO_2 may abstract an H-atom from the amine in aqueous solutions. H-abstraction also occurs in the reaction of protonated and unprotonated amines with the OH radical in the aqueous phase. In aqueous solution, the intermediate amino radical resulting from H-abstraction will easily be protonated to give the amino radical cation ($R_2N^{+\bullet}H$). Further reaction of the radical cation with NO_2 leads to the nitramine. Therefore the nitration reaction can be written as:

$(CH_3)_2N^{+\bullet}H(aq)$ + $NO_2(aq)$ → DMN(aq) + $H^+(aq)$ (X)

The reaction is assumed to be fast and an upper limit rate constant of 1×10^4 $M^{-1}s^{-1}$ was estimated, in agreement with the highest first order rate constant found by Giamalva et al. (1987) for alkenes.

2.5.5 Summary of implemented nitrosation and nitration reactions

Table 8 displays the nitrosation and nitration reactions together with their rate constants as implemented in the model.

Table 8: Nitrosation and nitration reactions included in the model.

Reaction in the aqueous phase	**k (M^{-1} s^{-1})**	**Reference**
DMA + N_2O_3 → NDMA + HONO	$4.29x10^7$	Mirvish (1975)
TMA + N_2O_3 → 0.05 NDMA + 0.05 HONO + 0.95 $(CH_3)_2NCH_2$	$4.0x10^7$	Challis and Kyrtopoulos (1979)
DEA + N_2O_3 → NDELA + HONO	$1.29x10^7$	This work
TEA + N_2O_3 → 0.05 NDELA + 0.95 $(HOCH_2CH_2)_2NCH_2CHOH$ + 0.05 HONO	$3.14x10^5$	This work
MMA + N_2O_4 → 0.3 MMN + 0.7 CH_2NH_2 + 0.3 HONO	$4.0x10^7$	Challis and Kyrtopoulos (1979)
DMA + N_2O_4 → 0.4 NDMA + 0.4 DMN + 0.2 CH_3NHCH_2 + 0.4 HONO + 0.4 HNO_3	$4.0x10^7$	Challis and Kyrtopoulos (1979)
TMA + N_2O_4 → 0.05 NDMA + 0.05 DEN + 0.9 $(CH_3)_2NCH_2$ + 0.05 HONO + 0.05 HNO_3	$4.0x10^7$	Challis and Kyrtopoulos (1979)
MEA + N_2O_4 → 0.3 MEN + 0.7 NH_2CH_2CHOH + 0.3 HONO	$4.0x10^7$	Challis and Kyrtopoulos (1979)
DEA + N_2O_4 → 0.4 NDELA + 0.4 DEN + 0.2 $(HOCH_2CH_2)NHCH_2CHOH$ + 0.4 HONO + 0.4 HNO_3	$4.0x10^7$	Challis and Kyrtopoulos (1979)
TEA + N_2O_4 → 0.05 NDELA + 0.05 DEN + 0.9 $(HOCH_2CH_2)_2NCH_2CHOH$ + 0.05 HONO + 0.05 HNO_3	$4.0x10^7$	Challis and Kyrtopoulos (1979)
DMA + HONO → NDMA + H_2O	0.1	Weller et al. (2011)
DMA + NO_2^- → NDMA + OH^-	0.1	Weller et al. (2011)
DEA + HONO → NDELA + H_2O	0.1	Weller et al. (2011)
DEA + NO_2^- → NDELA + OH^-	0.1	Weller et al. (2011)
$(CH_3)_2N^+$*H + NO_2 → DMN + H^+	$1.0x10^4$	This work, estimate

Destruction of nitrosamines and nitramines

Loss reactions of nitrosamines and nitroamines in the aqueous phase that are included in the amine chemistry mechanism are summarized in Table 9. In the aqueous phase, nitrosamines and nitroamines readily react with the hydroxyl radical. Nitrosamines undergo photolysis in the aqueous phase. Likely products of the reaction with OH(aq) are formaldehyde and an aminium ion (or ammonium).

The photolysis of nitrosamines and nitramines was investigated experimentally as part of this study. Detailed experimental procedures and results are provided in the report "D4 - Technical report on experimental results". Photo degradation kinetics were obtained for NDELA and MEANNO2 and are included in table 1 of this report.

Additional work focused on the potential of nitrite, nitrate and organic matter to cause a screening effect in the photolysis of nitrosamines in the aqueous phase by absorbing photons in the same wavelength range. This would result in decreased photo decay and increased lifetimes. While nitrite and nitrate screening effect using atmospherically relevant concentration ranges caused an up to 50 % increase in lifetimes, it will have a small effect (10-20 %) in clean to moderately polluted clouds. The organic matter screening effect observed was far more substantial and even under moderate concentrations for fogs and clouds, the lifetimes were increased 2 to 3 fold. Under high organic matter concentrations, the photolysis was all but suppressed. These experimental results imply that for worst case scenarios, an absence of photolysis of nitrosamines and nitramines in the atmospheric aqueous phase has to be considered.

The experimental work performed within this project also showed no effect of pH on nitrosamine (NDMA) photolysis over an atmospherically relevant pH range (1.2-6.8). This is consistent with work by Plumlee and Reinhard (2007) and different form earlier studies (Stefan and Bolton, 2002).

The photolysis rate found in experiments for MEANNO2 was used for all nitroamines, as an upper limit value. Photolysis of nitrosamines in aqueous droplets occurs roughly a factor 3-6 slower than in the gas phase.

In addition, screening effects may shield the nitrosamines against photolysis. This light screening effect, resulting from a competing absorbance of photons can lead to a substantial decrease in actual photolysis and hence an increase in atmospheric lifetimes of nitrosamines. From an atmospheric and cloud chemistry perspective both inorganic species (nitrate, nitrite) as well as atmospheric organic matter can decrease observed photo decay rates. Hutchings et al. (2010) showed that in the presence of large amounts of nitrite, no degradation was occurring due to similar absorbance bands. Similar effects have been observed by Chen et al (2010) with the addition of natural organic matter to surface waters.

The photolysis rates given in Table 9 are therefore upper limit values of the aqueous photolysis process. The lower limit of the photolysis rate is zero.

Table 9: Loss reactions of nitrosamines and nitramines used in the model.

Reaction in the aqueous phase	**k (M^{-1} s^{-1}) or j(s^{-1})**	**Reference**
MMN + OH → NH_4^+ + HCHO + OH^- + NO_2	$5.44x10^8$	as DMN + OH
NDMA + OH → MMA^+ + HCHO + OH^- + NO	$4.5x10^8$	Lee et al. (2007b)
DMN + OH → MMA^+ + HCHO + OH^- + NO_2	$5.44x10^8$	Mezyk et al. (2006)
NMEA + OH → $CH_2NH_3^+$ + HCHO + OH^- + NO	$4.5x10^8$	as NDMA + OH
MEN + OH → $CH_2NH_3^+$ + HCHO + OH^- + NO_2	$5.44x10^8$	as DMN + OH
NDELA + OH → MEA^+ + 2 HCHO + OH^- + NO	$6.99x10^8$	Mezyk et al. (2006)
DEN + OH → MEA^+ + 2 HCHO + OH^- + NO_2	$8.67x10^8$	Mezyk et al. (2006)
NDMA + hv → NO + $(CH_3)_2NH^+$ + OH^-	0.13*j(NO_2(g))	Chen et al. (2010)
NDELA + hv → NO + $(HOCH_2CH_2)_2NH^+$ + OH^-	0.053*j(NO_2(g))	This work
NMEA + hv → NO + $HOCH_2CH_2NH_2^+$ + OH^-	0.13*j(NO_2(g))	as NDMA + hv
MMN + hv → NO_2 + $CH_3NH_2^+$ + OH^-	$5.3x10^{-3}$*j(NO_2(g))	as MEN + hv
DMN + hv → NO_2 + $(CH_3)_2NH^+$ + OH^-	$5.3x10^{-3}$*j(NO_2(g))	as MEN + hv
MEN + hv → NO_2 + $HOCH_2CH_2NH_2^+$ + OH^-	$5.3x10^{-3}$*j(NO_2(g))	This work
DEN + hv → NO_2 + $(HOCH_2CH_2)_2NH^+$ + OH^-	$5.3x10^{-3}$*j(NO_2(g))	as MEN + hv

2.6 Results from realistic model simulations

The following cases were studied with the updated box model for conditions corresponding to the atmospheric state of the Mongstad area:

Case 1: Only gas phase chemistry of amines, no aqueous phase present. This is the Reference case.

Case 2: Gas phase chemistry, partitioning of amines to fog /cloud, and aqueous phase chemistry of amines in fog / cloud; with allowing nitrosamines/nitroamines to partition between the phases. This case results the most realistic description.

Case 3: Gas phase chemistry, partitioning of amines to fog /cloud, and aqueous phase chemistry of amines in fog / cloud; not allowing nitrosamines/nitroamines to partition between the phases.

Case 4: Gas phase chemistry, partitioning of amines to fog /cloud, and aqueous phase chemistry of amines in fog / cloud; not allowing nitrosamines/nitroamines to partition between the phases. No loss of nitrosamines/nitroamines in the aqueous phase.

Comparison of case 1 and case 2 will provide conclusions about the relevance of fog / cloud as a sink of gaseous amines and oxidation products. Case 1 is the reference simulation.

Comparison of aqueous phase concentrations from case 2 and case 3 (or case 4) will provide conclusions about the relevance of aqueous phase production of nitrosamines / nitroamines in fog and cloud. Case 4 will provide maximum aqueous phase concentrations in fog / cloud due to aqueous phase nitrosation / nitration.

Comparison of case 3 and case 4 will provide conclusions about the relevance of aqueous phase loss reactions for nitrosamines and nitroamines.

2.6.1 Conditions of the realistic simulations

Realistic simulations were performed with the zero-dimensional box model MAFOR for the photochemical and meteorological conditions typical for the Mongstad area which is best described as moderately polluted marine boundary layer. In this work, monthly average concentrations of pollutants and other atmospheric constituents were considered; higher pollution by VOCs and NO_x are likely directly in the industrial area (refinery) or during certain time periods. The investigation of pollution events at Mongstad or the chemistry inside the plume of the plant is out of the scope of this study.

Emission rate of all amines were estimated based on modelled maximum concentrations of MEA obtained in the worst case scenario calculations with TAPM (Karl et al., 2011a). For simplicity and to achieve unambiguous response from the model, emission of amines was assumed to occur continuously and to occur only in the gas phase. The emitted amount was identical for the different amines (not depending on vapour pressure) and for different seasons of the year. The initial concentration of amines in the gas phase was set to 250 pptv (6.5×10^9 molecules cm^{-3}) and the emission rate was derived from a case 1 simulation (only gas phase) of the scenario NNWJJA for MEA such that diurnal maximum concentrations of MEA during the 3-day simulation were 250 pptv. It is noted that for amines which are only capture process by-products, e.g. DMA, this is an overestimate of the actual emissions. Amines were allowed to react in the gas phase with OH radicals (amine + OH reaction) and/or partition to the aqueous phase of the fog. Other chemical reactions of amines in the gas phase were not considered. In the aqueous phase, amines were allowed to react with the aqueous OH radical and to participate in nitrosation and nitration reactions.

Continuous emissions of HONO from the ground surface were added and the emission rate was adjusted to produce maximum concentrations of 300 pptv HONO in the NNWJJA scenario (see Figure 12).

Model scenarios were defined for a simulation time of 3 days (72 hours) with a fog cycle. Each fog event started at 2 a.m. and ended at 10 a.m. (8 hours). LWC during fog was prescribed to the model as described in section 1.1. Fog formed at approximately 2 a.m. and fog dissipated at approximately 10 a.m. so that three full fog events were simulated. The simulations started at 5 a.m. of the first day in a fog period. By doing so, the chemical composition of fog droplets could be initialized with the aqueous phase concentrations given in Table 3.

Eight scenarios were available for use in box modelling; representing the Mongstad area in four different seasons (MAM, JJA, SON, DJF) when marine air mass arrived from either northwest (NNW, 270°-360°) or south-southeast (SEW, 120°-210°). From the eight scenarios, two were selected for the detailed modelling and for the yield determination: NNWJJA and SEWDJF. NNWJJA is representative for summer, when Mongstad predominantly receives marine air masses from northwest directly from the Atlantic Ocean. SEWDJF is representative for winter, when Mongstad predominantly receives continentally influenced marine air masses from southern directions. The largely different actinic fluxes in summer and winter lead to very different photochemical conditions in the two scenarios and also the length of sunlit daytime in the two scenarios is extremely different (NNWJJA: 19 hours; SEWDJF: 6.5 hours).

2.6.2 Results for background chemistry at Mongstad

To properly represent the photochemical clear sky conditions at Mongstad, it is important that modelled concentrations of typical atmospheric oxidants in the gas phase and in the aqueous phase are comparable to typically observed concentrations in similar air masses (moderately polluted remote or marine air).

Modelled concentrations of atmospheric oxidants in scenario NNWJJA (mid-summer) are shown in Figure 12. Ozone (O_3) concentrations increase from about 40 ppbv to about 60 ppbv. Photolysis of ozone and the subsequent reaction of O^1D atoms with water vapour as well as the photolysis of HONO produces OH during the day (up to $2x10^7$ molecules cm^{-3}). Besides its high reactivity, the importance of OH for the self-cleansing capability of the atmosphere is largely due to the fact that many of the OH reactions result in the production of the hydroperoxy radical (HO_2) which in turn can react with other trace gas molecules to yield OH again. This cycle is only terminated by the self-reaction of HO_2 which results in the formation of hydrogen peroxide (H_2O_2). HO_2 concentrations in the simulation reached up to $5x10^8$ molecules cm^{-3}.

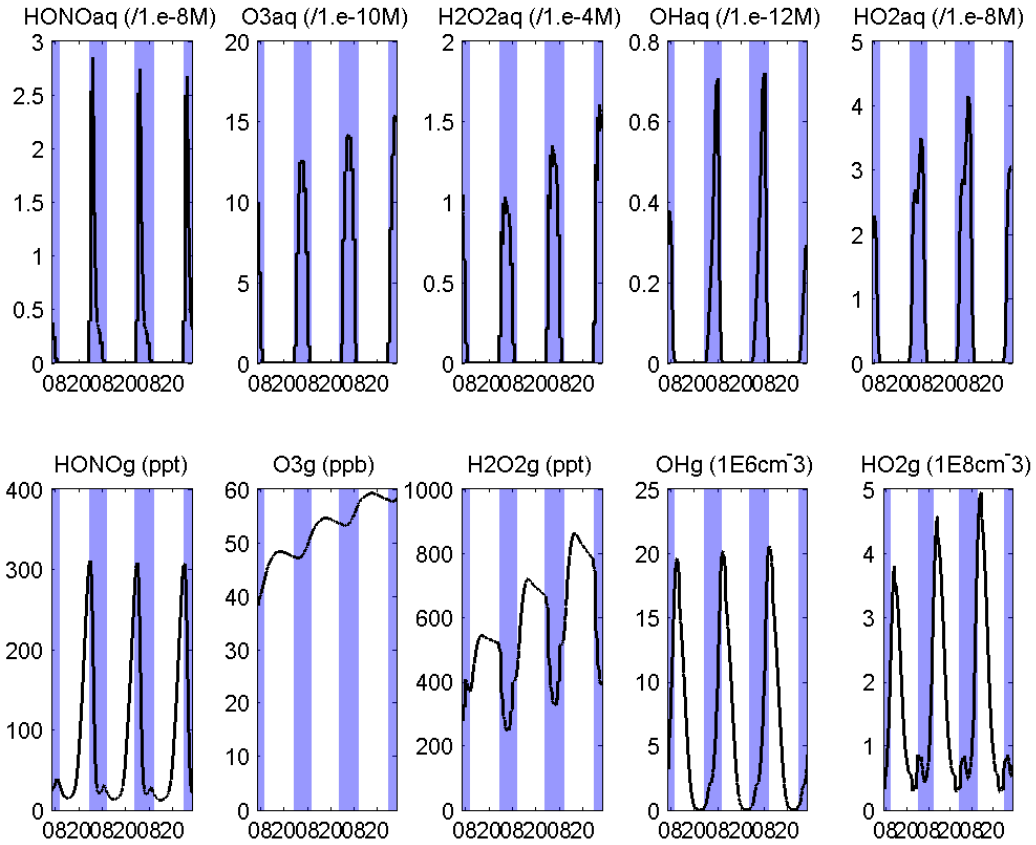

Figure 12: Modelled concentration time series of relevant oxidants in the aqueous phase (top panel) and gas phase (bottom panel) in scenario NNWJJA (case 4 simulation): nitrous acid (HONO), ozone (O_3), hydroxyl radical (OH) and hydroperoxy radical (HO_2). Fog periods are shaded in light blue.

All these gas phase constituents partition to a certain extent into the aqueous phase of fog. This is particularly clearly for the concentration time series of gaseous H_2O_2, which shows drops by several 100 pptv during fog periods. Aqueous phase concentrations of H_2O_2 reach levels of up to 0.15 mM in fog. Aqueous OH concentrations have a maximum at about 0.7×10^{-12} M which is in the same range but somewhat smaller than the maximum modelled OH(aq) concentrations of 1.9×10^{-12} M for a marine scenario reported by Hermann et al. (2000) using a higher LWC of 300 mg m^{-3}.

The concentration of nitrosating and nitrating reactants in the atmospheric aqueous phase will largely determine the relevance of particular nitrosation and nitration routes. Modelled concentrations of these reactants and of gaseous NO_x (dashed line: NO) shown in Figure 13.

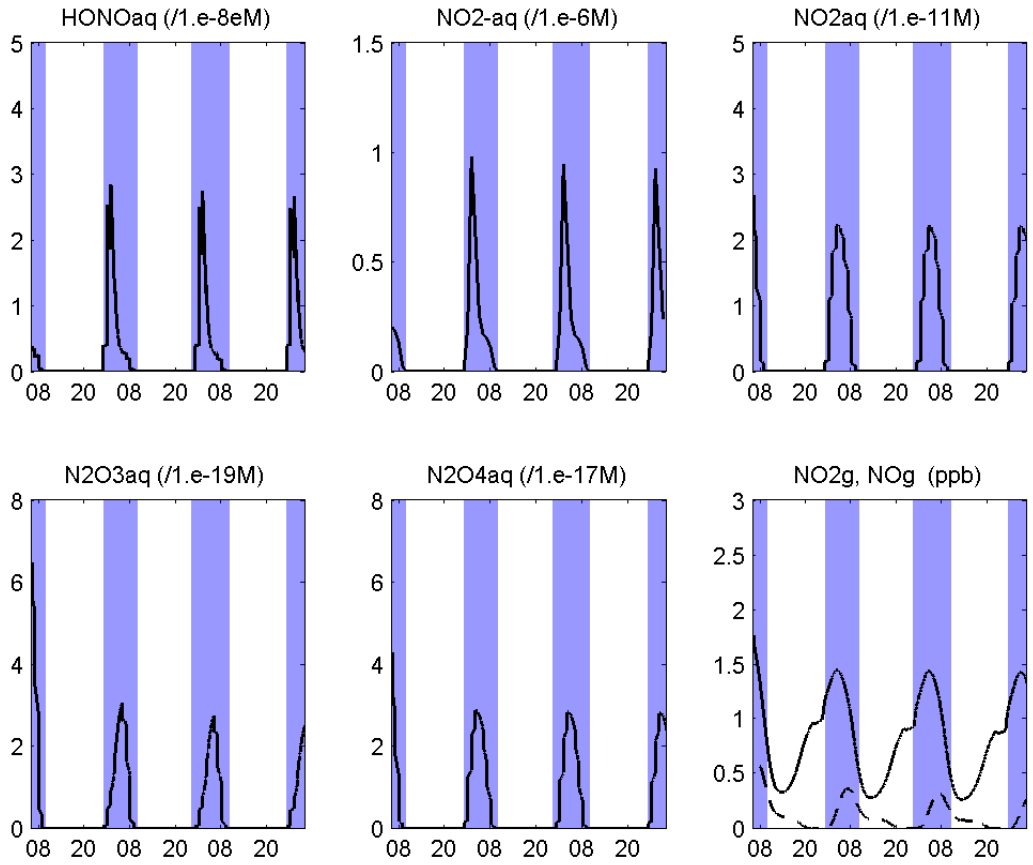

Figure 13: Modelled concentration time series of nitrosating and nitrating reactants in the aqueous phase (aq) and of gaseous NO_x compounds in scenario NNWJJA (case 4 simulation). Fog periods are shaded in light blue.

Nitrite (NO_2^-) is the most abundant of the nitrosating reactants with maximum concentrations of 1.0 µM. This nitrite concentration level is much smaller than typical levels observed in polluted fogs which are in the range of 5-130 µM (Herckes et al., 2007), but they are comparable to levels found in clouds (Acker et al., 2008). Nitrite concentrations observed in a variety of environments are shown in Figure 14. Nitrite typically results from the dissociation of HONO in the fog or cloud droplets (e.g. Lammel and Metzig, 1998; Acker et al., 2008).

Modelled maximum concentrations of aqueous N_2O_3 and N_2O_4 were 12 and 10 orders of magnitude smaller than those of NO_2^-, respectively. Total modelled NO_x mixing ratio in the gas phase peaked at ca. 2 ppbv. In the background atmosphere (distant from NO_x sources) the gaseous NO_2 mixing ratio is typically 2-5 times higher than the gaseous NO mixing ratio. Maximum aqueous NO_2 concentrations were $2x10^{-11}$ M and thus NO_2(aq) might be a relevant nitrating agent in droplets.

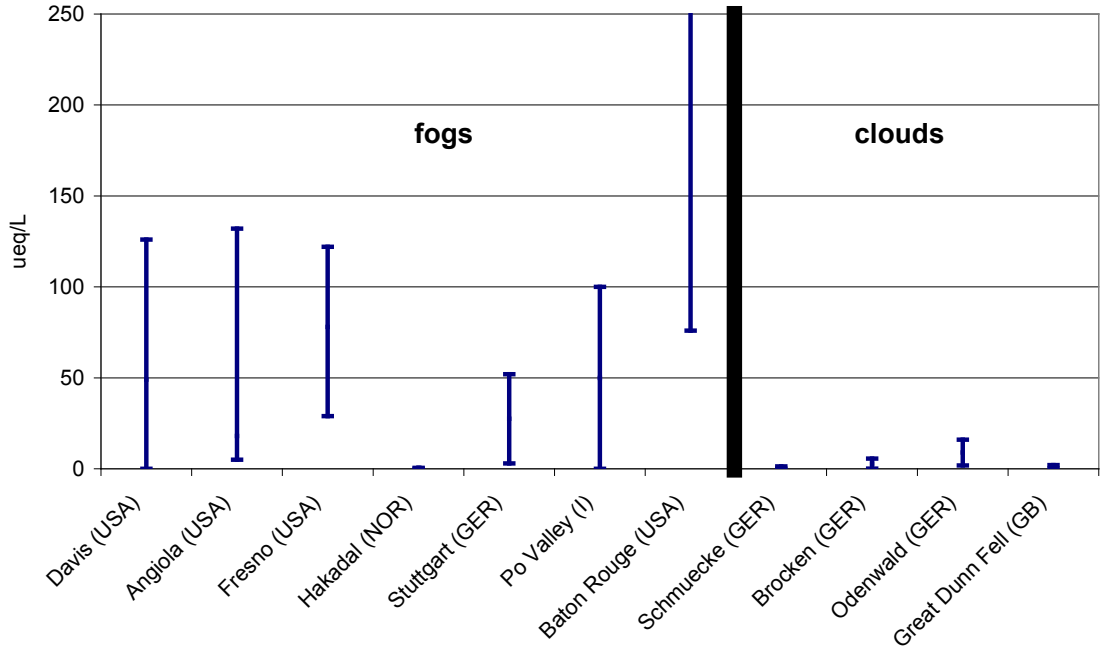

Figure 14: Nitrite concentrations as observed in the literature for fogs and clouds (unpublished; Herckes et al., 2007; Lammel and Metzig, 1998; Fuzzi et al., 1988; Acker et al., 2008; Cape et al., 1992).

2.6.3 Results for secondary amines (DMA and DEA)

The aqueous phase of fog and cloud is an important sink for gaseous amines (Figure 15). During fog periods gas phase concentrations of DMA were reduced by more than 80%. DEA gas phase concentrations during fog periods were essentially zero.

Mass transfer of gaseous amines and their oxidation products was treated in all simulation as given by equation (2) using a default value of 0.1 for the accommodation coefficient of all amine related compound. As described in section 1.2.5 the kinetics of the uptake to fog droplets were treated explicitly by the model in terms of forward and backward reaction. An equilibrium between gas phase and aqueous phase was however reached very quickly during the simulated fog periods.

Continuous emissions of DMA and DEA replenish their amounts in the gas phase each day of the simulation so that after the first day a steady state situation is reached.

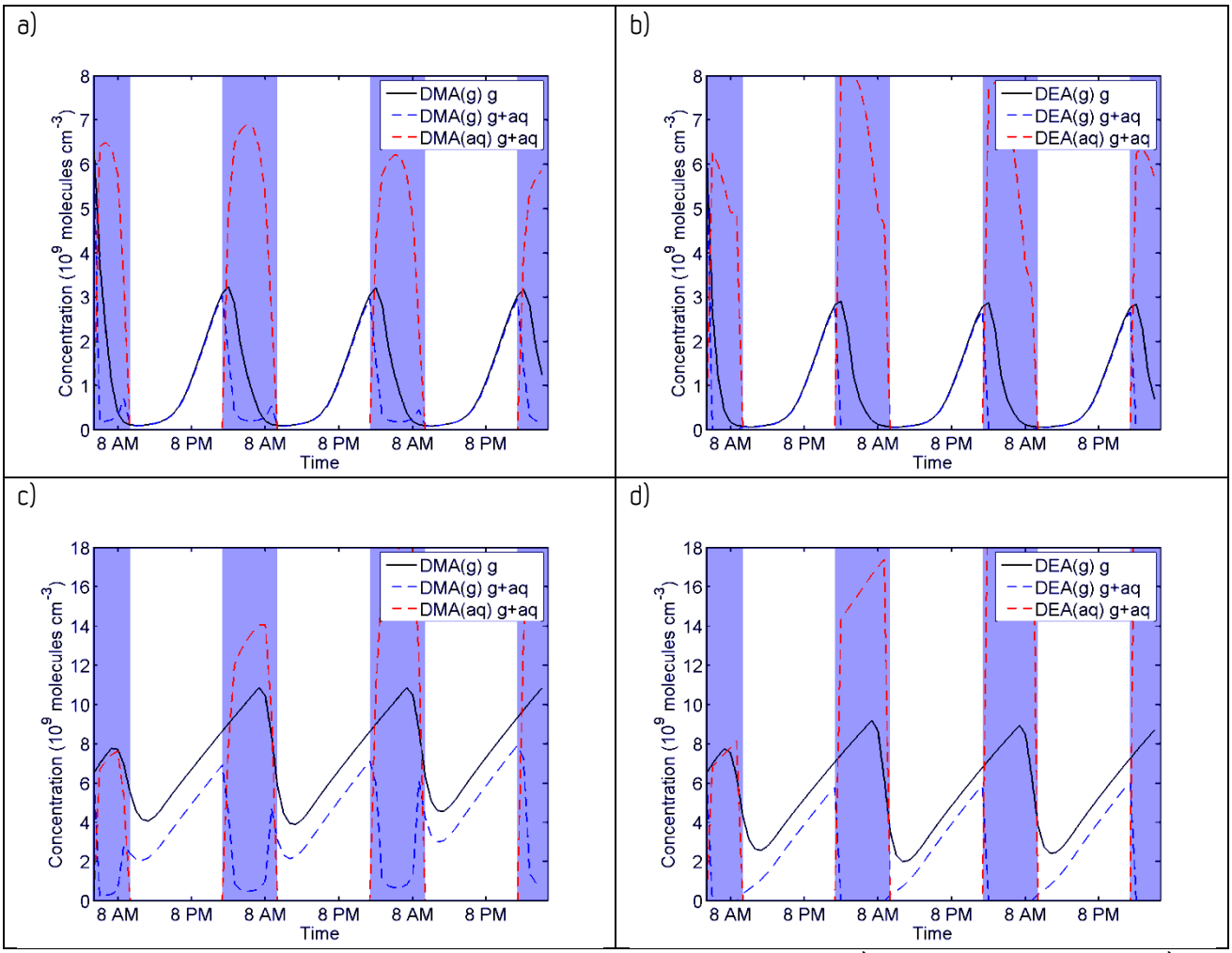

Figure 15: Secondary amines in realistic simulations for Mongstad conditions, a) DMA in scenario NNWJJA, b) DEA in scenario NNWJJA, c) DMA in scenario SEWDJF, d) DEA in scenario SEWDJF. Gas phase concentrations from reference simulation (case 1, "g" = gas phase only) are shown as black line, gas phase concentrations from case 2 ("g+aq" = all processes in gas phase and aqueous phase) are shown as red line, aqueous phase concentrations from case 2 are shown blue dashed line. Fog periods are shaded in light blue.

One assumption made in the modelling was that after fog dissipation the protonated amine (aminium) remains in the condensed phase and does not evaporate (see section 1.2.5). In the next fog event aqueous phase amine concentrations thus start at a level that remained from the previous fog period.

In summer (scenario NNWJJA), DEA reacted in aqueous solution relatively rapidly with OH(aq) leading to a decline of DEA(aq) by several 10^9 molecules cm^{-3}(air) during the 8 hour fog period (red dashed line). In winter, aqueous OH reaction was suppressed and both DMA and DEA concentrations in the aqueous phase increased during the fog period due to continued emissions.

In winter (scenario SEWDJF), the decay of gaseous DMA and DEA by OH radicals was much slower and minimum daytime concentrations of DMA and DEA were about $4x10^9$ molecules cm^{-3} and $2x10^9$ molecules cm^{-3}, respectively (case 1, "g"), much higher than in summer (<0.2 $x10^9$ molecules cm^{-3}). Maximum OH in winter was calculated to be $2x10^6$ radicals cm^{-3}.

2.6.4 Results for secondary nitrosamines (NDMA, NDELA)

Due to rapid photolysis during daytime, the gas phase concentrations of nitrosamines were lowest during the day. During the night, gaseous nitrosamines reached highest concentrations because of nitrosamine produced in the evening hours at reduced actinic flux. In winter there are only 6.5 hours with sunlight and NDMA tends to accumulate in the gas phase (Figure 16).

In scenario NNWJJA, maximum gas phase concentrations of NDELA in case 2 ("g+aq") were about a factor of 30 smaller than maximum gas phase concentrations of NDELA in case 1 ("g"). In scenario SEWDJF, maximum gas phase concentrations of NDELA in case 2 ("g+aq") were about a factor of 5 smaller than maximum gas phase concentrations of NDELA in case 1 ("g").

NDELA is completely partitioning to the aqueous phase during fog (K_H(NDELA) = $1x10^7$ M atm^{-1}), i.e. conditions of 100% partitioning are fulfilled for NDELA. In SEWDJF, modelled concentrations in case 2 ("g+aq") of NDELA(aq) are a factor of two larger than the concentrations of NDELA(g) before the fog events. This is due to continued emissions of DEA and gas production of NDELA in fog.

Aqueous phase in-situ production of NDELA by nitrosation of DEA(aq) contributed at most 10 % to the aqueous phase concentrations of NDELA in summer. When taking into account the loss of NDELA(aq) due to photolysis and OH reaction in the aqueous phase, the contribution of in-situ production becomes negligible. In winter aqueous in-situ nitrosation contributed up to 60 % to NDELA(aq) concentrations. Aqueous nitrosation is minor contribution to NDELA(aq) in summer but a substantial contribution in winter to concentrations of NDELA(aq). A test run without DEA emissions showed that NDELA(aq) concentrations were equal to the NDELA(g) concentrations before fog, confirming that the mass balance for NDELA had been maintained during the simulations. This also demonstrates that possible production of NDELA in the aqueous phase has a marginal effect on total NDELA concentrations. In first approximation NDELA may be treated by 100% partitioning disregarding aqueous phase production. It is cautioned that for nitrosamines with slightly lower Henry's law constants than NDELA the effect of aqueous nitrosation should not be neglected.

For NDMA the situation is less clear due to its higher volatility (K_H(NDMA) = 275 M atm^{-1}) which results in partitioning of only a small fraction partitions into the aqueous phase of fog. During the fog at night, aqueous phase concentrations of NDMA can be entirely explained by in-situ production in the droplets if loss of NDMA in the aqueous phase is not taken into account (red line vs. dashed green line). In winter aqueous phase loss rates are much slower and NDMA(aq) can be readily explained by aqueous phase nitrosation.

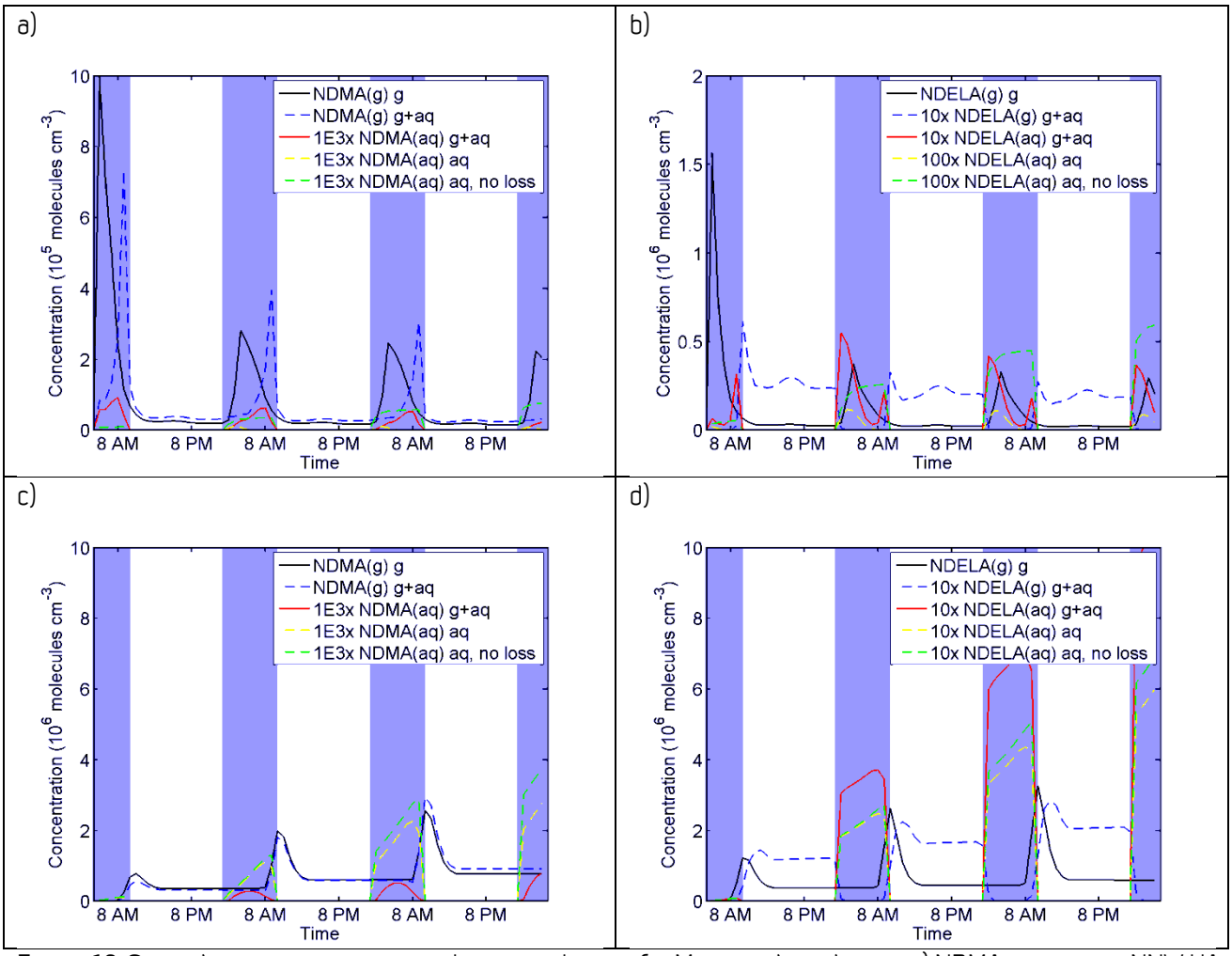

Figure 16: Secondary nitrosamines in realistic simulations for Mongstad conditions, a) NDMA in scenario NNWJJA, b) NDELA in scenario NNWJJA, c) NDMA in scenario SEWDJF, d) NDELA in scenario SEWDJF. Gas phase concentrations from reference simulation (case 1, "g" = gas phase only) are shown as black line, gas phase concentrations from case 2 ("g+aq" = all processes in gas phase and aqueous phase) are shown as red line, aqueous phase concentrations from case 2 (blue dashed line), case 3 (yellow dashed line), and case 4 (green dashed line) are also shown. Fog periods are shaded in light blue.

NDMA aqueous phase concentrations were about 3 orders of magnitude smaller than the NDMA gas phase concentrations. Therefore a possible approximation could be to neglect aqueous phase concentrations of NDMA since they are not significantly contributing to the total NDMA concentrations. However as noted above, concentration of NO_2^-(aq) can be 100 times higher in polluted fog (Herckes et al., 2007). Due to the high relevance of aqueous phase nitrosation of secondary amines by the 2nd order reaction with nitrite, 100 times higher nitrite concentrations are expected to translate into 100 times higher NDMA(aq) concentrations.

Aqueous concentrations of NDMA are also sensitive to a series of variables which affect the partitioning and the nitrosation reaction rate. In order to test the sensitivity of NDMA(aq) to different parameters (K_H, α, LWC, pH) a couple of sensitivity tests were performed based on simulations for case 2 (***Table 10***).

Table 10: Sensitivity of the average aqueous phase NDMA concentration towards changes of influential parameters in simulations with DMA in scenario NNWJJA.

Parameter	Default value	Test value	Ratio $NDMA(aq)_{test}$ / $NDMA(aq)_{default}$
Henry's law constant K_H(NDMA)	275 M atm^{-1}	862 M atm^{-1}	3.1
Accommodation coefficient α(NDMA)	0.1	1.0	1.0
LWC_{max}	106 mg m^{-3}	500 mg m^{-3}	0.9
pH	5.1	3.5	0.1

None of the tested changes in the parameters increased the average NDMA concentration in the aqueous phase more than by a factor of three which implies that NDMA(aq) is less than 1 % of the total NDMA concentration even when considering the uncertainties involved in modelling the partitioning between gas phase and aqueous phase and the nitrosation reaction rate. Increasing the Henry's law constant from 275 M atm^{-1} to 862 M atm^{-1} led to a proportional increase of NDMA(aq). Changing the accommodation coefficient of NDMA from 0.1 to 1.0 did not change resulting NDMA(aq). This is in line with the general observation that the establishment of the Henry's law equilibrium at the droplet interface is a rapid process both for insoluble and for soluble compounds with accommodation coefficients ≥0.1 (Seinfeld and Pandis, 1998). Increasing LWC_{max} of fog from about 100 mg m^{-3} up to 500 mg m^{-3} only had a minor effect on NDMA(aq) probably because loss of NDMA in the aqueous phase was taken into account in the test calculations. Finally, decreasing the pH value of fog from 5.1 to 3.5 reduced NDMA(aq) by a factor of 10. Decreasing pH further shifts the acid-base equilibrium of DMA to the side of the protonated form leaving less unprotonated DMA for the nitrosation reactions. Based on these tests, NDMA may be treated as pure gas phase compound with respect to estimating environmental effects. It is emphasized that this simplification does not hold for atmospheric situations with enhanced nitrite concentrations in fog droplets or pollution events with higher NO_x levels.

2.6.5 Results for secondary nitroamines (DMN, DEN)

The reduction of gas phase concentrations of amines during fog periods due to their uptake into the aqueous phase consequently led to a reduction of the gas phase production of nitroamines (black line vs. blue dashed line, Figure 17). Due to the relative low reactivity of gas phase nitroamines towards OH they were found to accumulate during daytime in summer. The much lower OH levels in winter and the shorter period of sunlight during the day enabled the accumulation of nitroamines during the simulation period, with gas phase DMN increasing up to $1x10^8$ molecules cm^{-3}.

For both DMN and DEN aqueous phase in-situ production contributed less than 1 % to the modelled aqueous phase concentration. It is concluded that nitration in the atmospheric aqueous phase of fog and cloud is an insignificant process.

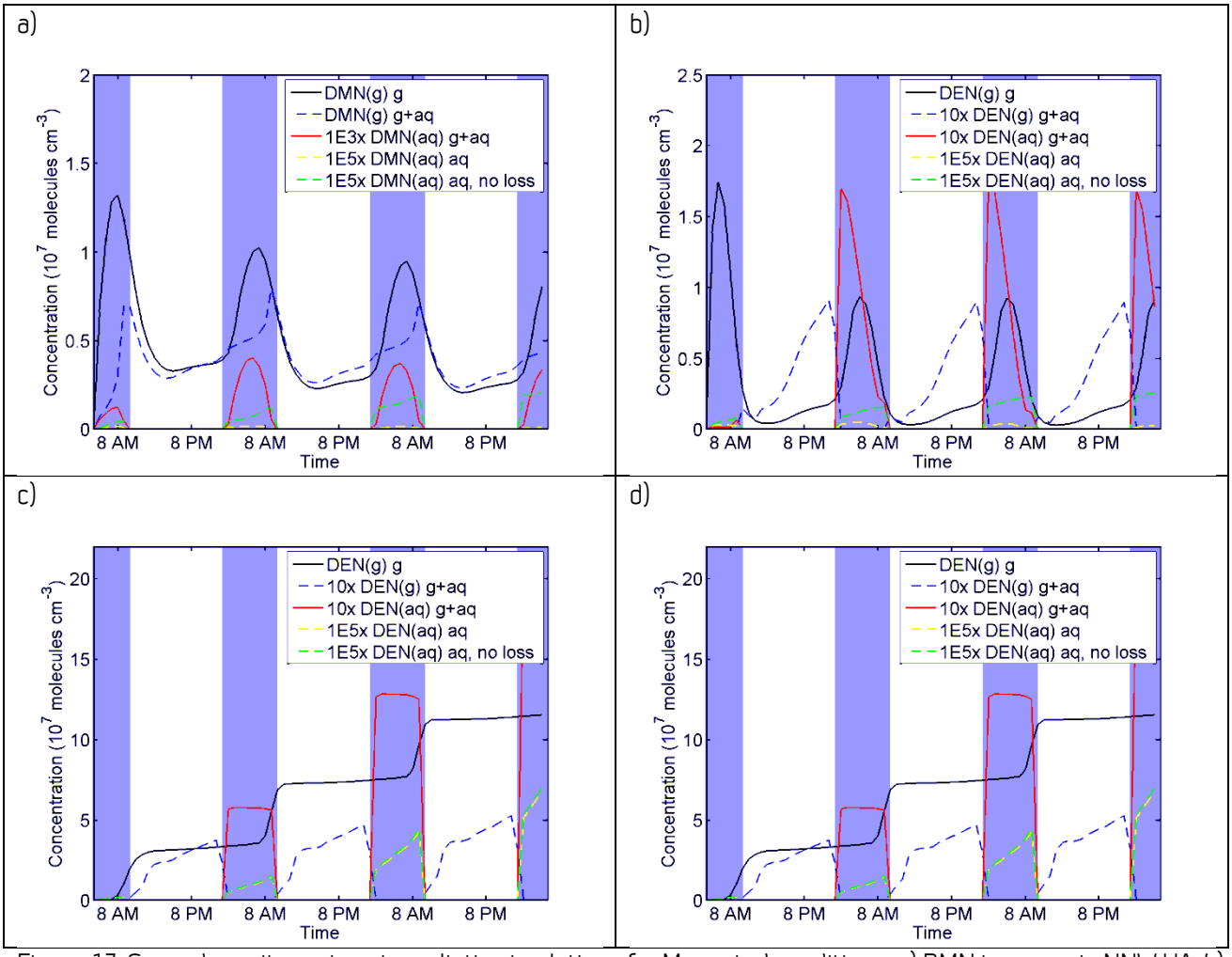

Figure 17: Secondary nitroamines in realistic simulations for Mongstad conditions, a) DMN in scenario NNWJJA, b) DEN in scenario NNWJJA, c) DMN in scenario SEWDJF, d) DEN in scenario SEWDJF. Gas phase concentrations from reference simulation (case 1, "g" = gas phase only) are shown as black line, gas phase concentrations from case 2 ("g+aq" = all processes in gas phase and aqueous phase) are shown as red line, aqueous phase concentrations from case 2 (blue dashed line), case 3 (yellow dashed line), and case 4 (green dashed line) are also shown. Fog periods are shaded in light blue.

Resulting concentrations of DMN in the aqueous phase were three orders of magnitude smaller than in the gas phase. Therefore DMN may be treated as pure gas phase compound with respect to estimating environmental effects.

Maximum gas phase concentrations of DEN for case 2 ("g+aq") were about a factor of 7 smaller than maximum gas phase concentrations of DEN in case 1 ("g"). DEN is completely partitioning into the aqueous phase during fog (K_H(DEN) = **2.37x10**^{9} M atm^{-1}). Therefore DEN may be treated by 100% partitioning disregarding aqueous phase nitration.

2.6.6 Rates of aqueous phase production and destruction processes

Production and destruction rates of NDMA in the aqueous phase were analyzed for scenario NNWJJA and scenario SEWDJF from model simulations of case 2 ("g+aq"). Total production rate of NDMA is about two orders of magnitude larger in winter than in summer (Figure 18). More than 99% of the total production rate of NDMA is explained by the 2nd order nitrosation reaction, i.e. nitrosation 1st order in nitrite (dashed black line coincides with blue line). The production rate of 3rd order nitrosation is three orders of magnitude smaller than the production rate of 2nd order nitrosation. The reaction of DMA with N_2O_4 produced about 20 times more NDMA than the reaction of DMA with N_2O_3.

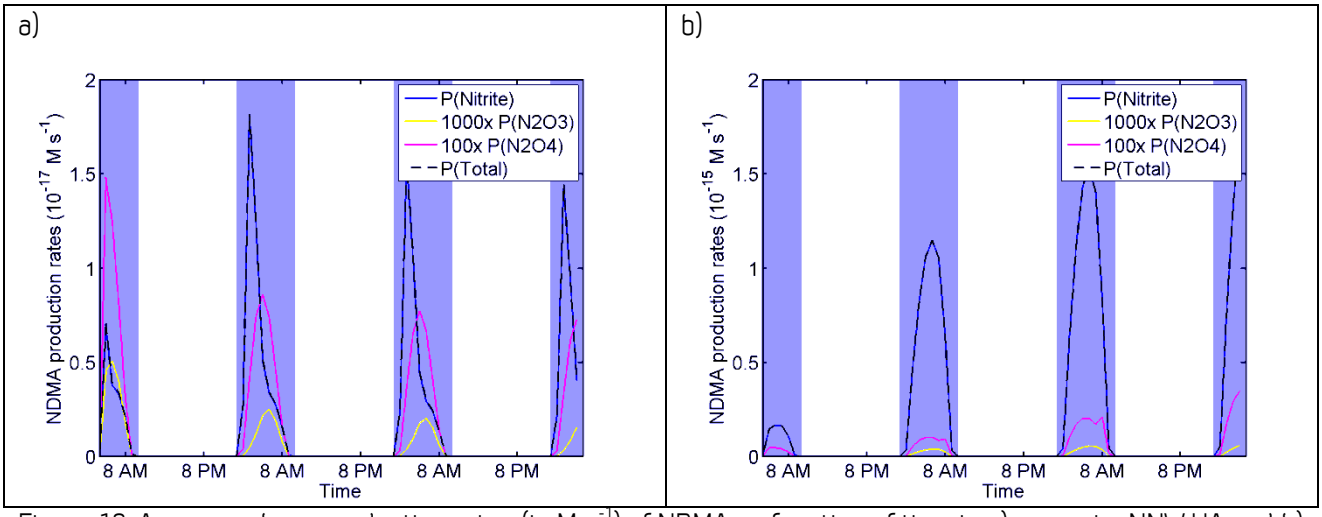

Figure 18: Aqueous phase production rates (in M s^{-1}) of NDMA as function of time in a) scenario NNWJJA and b) scenario SEWDJF. Blue line: 2nd order nitrosation by nitrite, magenta line: nitrosation by N_2O_4 scaled by a factor of 100, yellow line: nitrosation by N_2O_3 (3rd order nitrosation) scaled by a factor of 1000, dashed black line: total production. The blue line coincides with the dashed black line, indicating that the total production rate is almost completely explained by 2nd order nitrosation. Note the different order of magnitude of the y-axis for NNWJJA (10^{-17} M s^{-1}) and SEWDJF (10^{-15} M s^{-1}).

Total production rate of NDELA in the aqueous phase was about two orders greater than that of NDMA. Also for NDELA, more than 99% of the total production rate of NDMA is explained by the 2nd order nitrosation reaction, i.e. nitrosation 1st order in nitrite. The relevance of the N_2O_3 and N_2O_4 productions reactions was similar to that found for NDMA.

From this analysis it is concluded that the aqueous phase production of NDMA and NDELA is determined by the rate expression for the 2nd order nitrosation reaction. It is noted that the corresponding rate expression was not derived in this work, but adopted from the work of Weller et al. (2011) as described in section **1.6.2**.

Maximum production rates of the nitrosamines (NDMA and NDELA), and the nitroamines (DMN and of DEN) are summarized in **Table 11** for scenario NNWJJA and in **Table 12** for scenario SEWDJF. In summer the production of DMN by reaction of the DMA radical cation with NO_2 was twice the production by nitration with N_2O_4. In winter the production of DMN by N_2O_4 was more important than the production by NO_2. A corresponding nitration reaction with NO_2 was not included for DEN, and the only reaction producing DEN was the nitration reaction with N_2O_4.

Table 11: Maximum production rates for NDMA, NDELA, DMN and DEN (in 10^{-16} M s^{-1}) for the respective nitrosation and nitration pathways in scenario NNWJJA.

Compound	NDMA	DMN	NDELA	DEN
2^{nd} order nitrosation (1^{st} order in nitrite)	6.63	—	1445	—
Reaction with N_2O_4	0.035	0.035	8.14	8.14
Reaction with N_2O_3	0.001	—	0.077	—
Nitration with NO_2	—	0.077	—	—

Table 12: Maximum production rates for NDMA, NDELA, DMN and DEN (in 10^{-16} M s^{-1}) for the respective nitrosation and nitration pathways in scenario SEWDJF.

Compound	NDMA	DMN	NDELA	DEN
2^{nd} order nitrosation (1^{st} order in nitrite)	35.35	—	36016	—
Reaction with N_2O_4	0.084	0.084	19.21	19.21
Reaction with N_2O_3	0.002	—	0.172	—
Nitration with NO_2	—	0.015	—	—

The destruction of NDMA in the aqueous phase was dominated by photolysis. The loss by reaction with OH(aq) was a factor 4-6 smaller than the loss by photolysis both in summer and winter. The aqueous phase loss was on average about 50 times faster in summer than in winter. The destruction rate of the NDMA + OH reaction was on average $2.9x10^{-5}$ s^{-1} and $7.2x10^{-7}$ s^{-1} in NNWJJA and SEWDJF, respectively. The destruction rate of NDMA + hν was on average $1.7x10^{-4}$ s^{-1} and $2.8x10^{-6}$ s^{-1} in NNWJJA and SEWDJF, respectively.

The destruction of NDELA in the aqueous phase was dominated by photolysis. The loss by reaction with OH(aq) was a factor 2-4 smaller than the loss by photolysis both in summer and winter. The aqueous phase loss was on average about 60 times faster in summer than in winter. The destruction rate of the NDELA + OH reaction was on average $1.6x10^{-5}$ s^{-1} and $6.7x10^{-7}$ s^{-1} in NNWJJA and SEWDJF, respectively. The destruction rate of NDELA + hν was on average $7.0x10^{-5}$ s^{-1} and $1.2x10^{-6}$ s^{-1} in NNWJJA and SEWDJF, respectively.

2.7 Maximum yields of nitrosamines and nitramines

2.7.1 Procedure to determine production yields

In the model runs to determine yields of nitrosamines and nitroamines no emissions of amines were added. Gas phase production yields were determined from the first hour of the model simulation with no fog (between 5 a.m. and 6 a.m. local time, Mongstad). Aqueous phase yields were determined from one hour fog (between 6 a.m. and 7 a.m. local time, Mongstad). All concentrations (gas phase and aqueous phase) used for the yield calculation are given in units molec cm^{-3}.

Yields of nitrosamines and nitroamines in the gas phase production were determined as the slope of the plot of nitrosamine or nitramine concentration versus amine reacted (all in units molecules cm^{-3}), by linear regression. The slope of the regression line is defined by:

$$Y_g(\%) = \frac{\Delta[\text{Product}(t)]_g}{\Delta[\text{Amine}(t_0) - \text{Amine}(t)]_g} \cdot 100\% \qquad (11)$$

Where [Amine(t_0)] is the initial concentration of amine in the gas phase (i.e. t_0 = 0). Figure 19 shows the yield plots for DMA gas phase oxidation. Figure 19 a) shows the yield curve obtained for dimethylnitramine (DMN) and Figure 19 b) shows the yield curve for N-nitrosodimethylamine (NDMA). While DMN shows a clear linear relation with the reacted amine, NDMA depends strongly on the actinic flux and due to variation in the solar radiation only a weak linear relationship with the reacted amine can be expected.

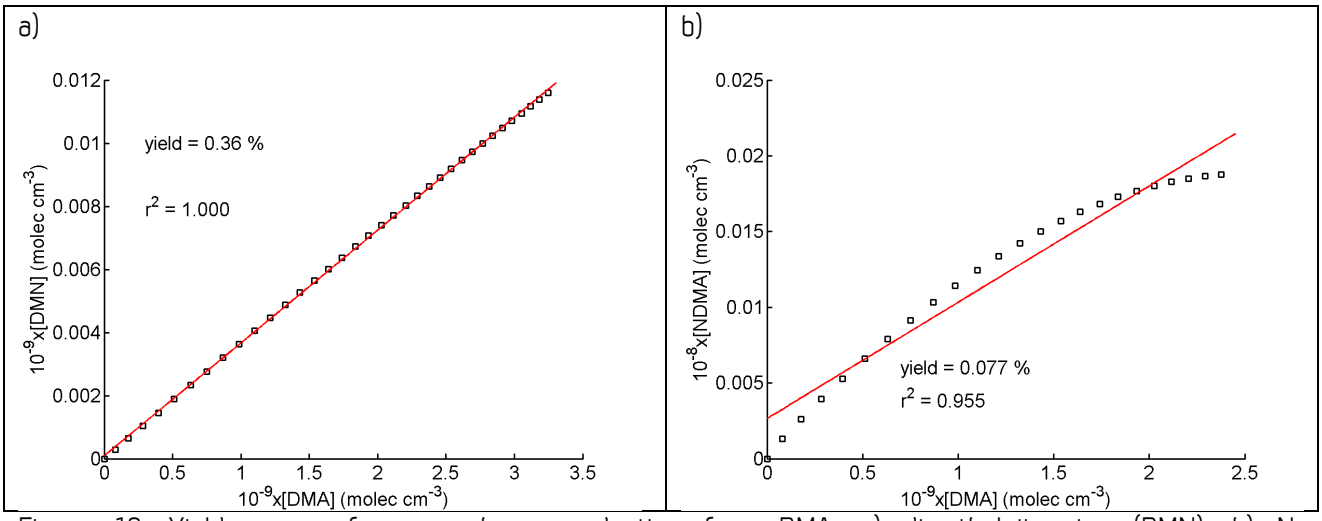

Figure 19: Yield curves for gas phase production from DMA: a) dimethylnitramine (DMN), b) N-nitrosodimethylamine (NDMA). The yields are determined from the slopes by linear regression to the yield curves (red lines).

Yields of nitrosamines and nitroamines in the aqueous phase production were calculated for a fog with a constant LWC of 100 mg m^{-3} and pH = 5. The derived yields are strictly only valid for these conditions.

For the aqueous phase, two different yields were calculated: 1) the total aqueous phase yield due to partitioning from the gas phase and in-situ aqueous phase production and 2) the aqueous phase production yield alone. The yields for the aqueous phase are computed from the model runs without loss reactions in the aqueous phase, and thus are *maximum yields*.

The (in-situ) aqueous phase production yield, $Y_{aq,prod}$, is calculated from a model run that did not allow for partitioning of nitrosamines and nitroamines between gas phase and aqueous phase as the slope of the plot of nitrosamine or nitramine concentration versus amine reacted in the aqueous phase (all in units molecules cm^{-3}), by linear regression. The slope of the regression line is defined by:

$$Y_{aqprod}(\%) = \frac{\Delta[\text{Product}(t)]_{aq}}{\Delta[\text{Amine}(t_f) - \text{Amine}(t)]_{aq}} \cdot 100\% \qquad (12)$$

Where [Amine(t_f)] is the concentration of amine at the beginning of the fog. Figure 20 a) shows the yield curve obtained for DMN and Figure 20 b) shows the yield curve for NDMA from DMA aqueous phase oxidation. While DMN shows a clear linear relation with the reacted amine, NDMA depends on the partitioning of nitrosating reactants (e.g. HONO) from the gas phase into the aqueous phase and therefore a weaker linear relationship.

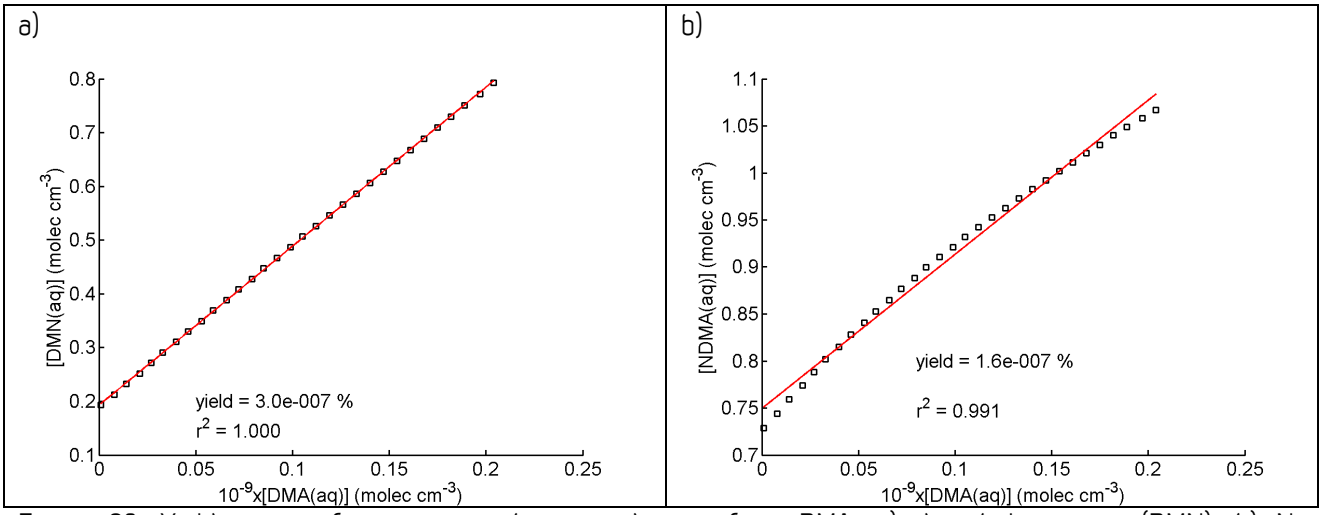

Figure 20: Yield curves for aqueous phase production from DMA: a) dimethylnitramine (DMN), b) N-nitrosodimethylamine (NDMA). The yields are determined from the slopes by linear regression to the yield curves (red lines).

The total aqueous phase yield, $Y_{aq,tot}$, is calculated from a model run that allowed for partitioning of nitrosamines and nitroamines between gas phase and aqueous phase. Since partitioning is not a production term in a strict sense, yields were estimated by using the maximum product concentration in the aqueous phase:

$$Y_{aqtot}(\%) = \frac{\max\left([\text{Product}(t)]_{aq}\right)}{[\text{Amine}(t_f) - \text{Amine}(t_e)]_{aq}} \cdot 100\% \qquad (13)$$

Where [Amine(t_e)] is the concentration of amine after one hour of fog.

2.7.2 Summary of production yields

Yields for the gas phase and the aqueous phase were determined using Eq. (11) - (13). The product yields of nitrosamines and nitroamines are summarized in Table 13 for scenario NNWJJA (summer) and in Table 14 for scenario SEWDJF (winter).

In summer, gas phase product yields for nitrosamines ranged from 0.004 % to 0.08 % and gas phase product yields for nitramines range from 0.08 % to 0.5 %. In winter, gas phase product yields for nitrosamines ranged from 0.0001 % to 0.003 % and gas phase product yields for nitramines range from 0.07 % to 0.4 %. Gas phase product yields of nitrosamines and nitramines increase in the order primary < secondary < tertiary amine. It is noted that the nitrosamine of MEA has not been detected in chamber experiments until now and the given yield is an upper limit value.

Table 13: Maximum product yields of nitrosamines and nitramines from methylamines and ethanolamines in the gas phase and in the aqueous phase for scenario NNWJJA.

Compound	Yg (%) nitrosamines	Yaq,prod (%) nitrosamines	Yaq,tot (%) nitrosamines	Yg (%) nitramines	Yaq,prod (%) nitramines	Yaq,tot (%) nitramines
Monomethylamine	—	—	—	0.13	$8x10^{-9}$	0.0006
Dimethylamine	0.077	$2x10^{-7}$	0.0004	0.36	$3x10^{-7}$	0.0043
Trimethylamine	0.118	$2x10^{-9}$	0.0003	0.53	$2x10^{-9}$	0.0030
Monoethanolamine	0.004	—	0.013	0.08	$5x10^{-8}$	0.203
Diethanolamine	0.033	$3x10^{-6}$	0.264	0.34	$9x10^{-8}$	2.210
Triethanolamine	0.047	$2x10^{-7}$	0.283	0.43	$2x10^{-7}$	2.535

Table 14: Maximum product yields of nitrosamines and nitramines from methylamines and ethanolamines in the gas phase and in the aqueous phase for scenario SEWDJF.

Compound	Yg (%) nitrosamines	Yaq,prod (%) nitrosamines	Yaq,tot (%) nitrosamines	Yg (%) nitramines	Yaq,prod (%) nitramines	Yaq,tot (%) nitramines
Monomethylamine	—	—	—	0.11	$3x10^{-8}$	$1x10^{-5}$
Dimethylamine	0.0016	$1x10^{-5}$	$7x10^{-7}$	0.39	$6x10^{-7}$	0.0002
Trimethylamine	0.0009	n.d. [1]	n.d. [1]	0.14	n.d. [1]	n.d. [1]
Monoethanolamine	0.0001	—	$7x10^{-6}$	0.07	$3x10^{-7}$	0.0017
Diethanolamine	0.0022	0.0002	0.0008	0.17	$9x10^{-7}$	0.0155
Triethanolamine	0.0031	$1x10^{-5}$	0.0003	0.21	$1x10^{-5}$	0.0296

[1] n.d.: not possible to derive yields because $[Amine(t_e)]_{aq} > [Amine(t_f)]_{aq}$..

Aqueous phase product yields ($Y_{aq,prod}$) of nitrosamines ranged from $2x10^{-9}$ % to $3x10^{-6}$ % and aqueous phase product yields of nitramines ranged from $2x10^{-9}$ % to $3x10^{-7}$ %. In winter aqueous phase product yields are 1-2 orders of magnitude larger because the level of nitrosating and nitrating agents in the aqueous phase is higher. Aqueous phase product yields of nitrosamines are 5 to 7 orders of magnitude smaller than the corresponding gas phase product yields. Aqueous phase product yields of nitramines are 6 to 8 orders of magnitude smaller than the corresponding gas phase product yields. Aqueous phase product yields of nitrosamines are highest for secondary amines. No nitrosamines are formed in the aqueous phase oxidation of primary amines. Since nitrosamines and nitramines are only formed in the nitrosation/nitration reaction of the unprotonated amine in the aqueous phase, the product yields also depend on the fraction of the unprotonated form.

Total yields for the aqueous phase ($Y_{aq,tot}$), which include partitioning of gas phase nitrosamines and nitramines into the aqueous phase, may be used in atmospheric dispersion modelling to estimate the maximum concentrations of nitrosamines and nitramines in the aqueous phase without detailed description of the partitioning and nitrosation/nitration reactions (only partitioning of amines to the aqueous phase needs to be described). Total aqueous phase yields of nitrosamines ranged from 0.0003 % to 0.28 % in summer. Total aqueous phase yields of nitramines ranged from 0.0006 % to 0.003 % for methylamines and from 0.2 % to 2.5 % for ethanolamines in summer. In winter total aqueous phase yields are about 3 orders of magnitude smaller. For ethanolamines, the total yields in the aqueous phase are dominated by the partitioning of gaseous nitrosamines and nitramines; in-situ aqueous phase production being a negligible contribution to the amount in the aqueous phase.

$Y_{aq,tot}$ strongly depends on the magnitude of the uptake of the nitrosamines/nitramines into the aqueous phase defined by their Henry's law constants. Reliable partitioning data is thus crucial for the correct estimation of total yields $Y_{aq,tot}$. For DMA and TEA the effect of using different K_H data was tested. For TEA the use of K_H(TEA) = $3.05x10^4$ M atm^{-1} estimated by SM8 resulted in $Y_{aq,tot}$(NDELA) = 0.599 % and $Y_{aq,tot}$(DEN) = 5.983 % in scenario NNWJJA, and thus almost doubled compared to the original K_H(TEA) = $\mathbf{1.42x10^9}$ given by Ge et al. (2011). The difference can be explained by increased gas phase production due to reduced loss of gaseous TEA to the aqueous phase. For DMA changing the K_H value of NDMA from 275 M atm^{-1} to 862 M atm^{-1} (estimated by SM8) resulted in a near proportional increase of the total yield ($Y_{aq,tot}$(NDMA) = 0.0013 %) in scenario NNWJJA.

2.8 Conclusions from the model study

- The aqueous phase of fog and cloud is an *important sink for gaseous amines*. During fog periods gas phase concentrations of DMA and DEA were reduced by more than 80%. Partitioning of amines to the aqueous phase has to be based on the *effective Henry's law coefficient, K_H^{eff}, which takes into account acid-base dissociation of amines (i.e. their pK_a).*
- Due to rapid photolysis during daytime, the gas phase concentrations of nitrosamines were lowest during the day. During the night, gaseous nitrosamines reached highest concentrations because of nitrosamine produced in the evening hours at reduced actinic flux. In winter gaseous nitrosamines were found accumulate in the atmosphere.
- In first approximation N-nitroso diethanolamine (NDELA) may be treated by 100% partitioning to the aqueous phase of fog and cloud, disregarding aqueous phase production. However, aqueous phase in-situ production of NDELA may contribute substantially to NDELA concentrations in fog and cloud droplets in winter. It is cautioned that for nitrosamines with slightly lower Henry's law constants than NDELA the effect of aqueous nitrosation should not be neglected.
- N-nitroso dimethylamine (NDMA) aqueous phase concentrations were about 3 orders of magnitude smaller than the NDMA gas phase concentrations. Even when considering the uncertainties involved in modelling the partitioning between gas phase and aqueous phase and the nitrosation reaction rate, NDMA(aq) contributed less than 1 % to the total NDMA concentrations.
- Based on several sensitivity tests, NDMA may be treated as pure gas phase compound with respect to estimating environmental effects. It is emphasized that this simplification does not hold for atmospheric situations with enhanced nitrite concentrations in fog droplets or pollution events with higher NO_x levels.
- Aqueous phase production of nitrosamines was dominated by the ^{2nd} order reaction, i.e. first order in nitrite. The rate expression used for the ^{2nd} order reaction was adopted from Weller et al. (2011). Not considering this reaction would turn aqueous nitrosation into an insignificant process in the atmosphere.
- Due to the relative low reactivity of gas phase nitroamines towards OH they accumulate in the atmosphere. *Nitration in the atmospheric aqueous phase of fog and cloud was found to be an insignificant process.* Dimethylnitramine (DMN) may be treated as pure gas phase compound with respect to estimating environmental effects. Diethanol nitramine (DEN) may be treated by 100% partitioning disregarding aqueous phase nitration.
- Chemical loss of nitrosamines and nitroamines in the aqueous phase by OH reaction and photolysis may be neglected to result a conservative estimate for environmental effects of emissions of amines. In winter these loss reactions are insignificant. The neglect of aqueous photolysis of nitrosamines and nitroamines is supported by experiments demonstrating that the screening effect of dissolved organics effectively prevents photolysis of these compounds.

References

Acker, K., Beysens, D., Moller, D. (2008). Nitrite in dew, fog, cloud and rain water - indicator for heterogeneous processes on surfaces. *Atmospheric Research*, 87, 200-212.

Anastasio, C. and Chu, L. (2009). Photochemistry of nitrous acid (HONO) and nitrous acidium ion (H_2ONO^+) in aqueous solution and ice. *Environ.Sci.Tech.*, 43, 1108-1114.

Angelino, S., Suess, D. T., Prather, K. A. (2001). Formation of aerosol particles from reactions of secondary and tertiary alkylamines: Characterization by aerosol time-of-flight mass spectrometry. *Environ. Sci. Technol.*, 35, 3130-3138.

Angove, D., Jackson, P., Lambropoulos, N., Azzi, M., Attalla, M. (2010). CO_2 Capture Mongstad – Project B - Theoretical evaluation of the potential to form and emit harmful compounds, CSIRO Report, available at: http://www.gassnova.no/frontend/files/CONTENT/Rapporter/AtmosphericFormation CSIRO.pdf.

Aumont, B., Chervier, F., Laval, S. (2003). Contribution of HONO sources to the $NO_x/HO_x/O_3$ chemistry in the polluted boundary layer. Atmos. Environ., 37, 487-498.

Bone, R. Cullis, P, Wolfenden, R. (1983). Solvent effects on equilibria of addition of nucleophiles to acetaldehyde and the hydrophilic character of diols. *J. Am. Chem. Soc.*, 105, 1339-1343.

Bråten, H. B., Bunkan, A. J., Bache-Andreassen, L., Solimannejad, M., and Nielsen, C. J. (2008). Final report on a theoretical study on the atmospheric degradation of selected amines. NILU OR 77/2008, Norwegian Institute for Air Research, Kjeller, Norway, available at: http://www.nilu.no.

Cape, J. N., Hargreaves, K. J., Storeton-West, R., Fowler, D., Colvile, R.N., Choularton, T. W., Gallagher, M. W. (1992). Nitrite in orographic cloud as an indicator of nitrous acid in rural air. *Atmospheric Environment*, 26A, 2301-2307.

Casado, J., Mosquera, M., Paz, L. C., Prieto,M. F., Tato, J. V. (1984). Nitrite ion as a nitrosating Reagent. Nitrosation of morpholine and diethylamine in the presence of formaldehyde. *J. Chem. Soc. Perkin Trans. II*, 1963-1966.

Challis, B. C. and Challis, J. A. (1982). N-nitrosamines and N-nitrosimines. Vol. 2, Ed. S. Patai, John Wiley and Sons, New York, pp. 1151-1223.

Challis, B. C.; Kyrtopoulos, S. A. (1979). Chemistry of nitroso-compounds. 11. Nitrosation of amines by the 2-phase interaction of amines in solution with gaseous oxides of nitrogen. *J. Chem. Soc. Perkin Trans. 1*, 2, 299-304.

Chen, B., Lee, W., Westerhoff, P. K., Krasner, S. W., Herckes, P. (2010). Solar photolysis kinetics of disinfection byproducts. *Water Research*, 44, 3401-3409.

Christie, A. O. and Crisp, D. J. (1967). Activity coefficients of n-primary, secondary and tertiary aliphatic amines in aqueous solution. *J. Appl. Chem. USSR*, 17, 11-14.

Cooney, R. V., Ross, P. D., Bartolini, G. L., Ramseyer, J. (1987). N-nitrosamine and N-nitroamine formation: Factors influencing the aqueous reactions of nitrogen dioxide with morpholine. *Environ. Sci. Technol.*, 21, 77-83.

Das, S. and von Sonntag, C. (1986). The oxidation of trimethylamine by OH radicals in aqueous solution, as studied by pulse radiolysis, ESR, and product analysis. The reactions of the alkylamine radical cation, the aminoalkyl radical, and the protonated aminoalkyl radical. *Z. Naturforschung*, 41B, 505-513.

Das, S., Schuchmann, M. N., Schuchmann, H.-P., von Sonntag, C. (1987). The production of the superoxide radical anion by the OH radical-induced oxidation of trimethylamine in oxygenated aqueous solution. The kinetics of the hydrolysis of (hydroxymethyl)dimethylamine. *Chem. Ber.,* 120, 319-323.

Ervens, B., George, C., Williams, J. E., Buxton, G. V., Salmon, G. A., Bydder, M., Wilkinson, F., Dentener, F., Mirabel, P., Wolke, R., Herrmann, H. (2003). CAPRAM2.4 (MODAC mechanism): An extended and condensed tropospheric aqueous phase mechanism and its application. *J. Geophys. Res.,* 108D, 4426, DOI 10.1029/2002JD002202.

Finlayson-Pitts, B. J. and Pitts, Jr., J. N. (2000). Chemistry of the Upper Lower Atmosphere. Theory, Experiments and Applications. Academic Press, San Diego.

Fuzzi, S., Orsi, G., Nardini, G., Facchini, M.-C., McLaren, S., McLaren, E., et al. (1988). Heterogeneous processes in the Po Valley radiation fog. *J. Geophys. Res.,* 93, 11141-11151.

Ge, X., Wexler, A. S., Clegg, S. L. (2011). Atmospheric amines - Part II: Thermodynamic properties and gas/particle partitioning. *Atmos. Environ.,* 45, 561-577.

Giamalva, D. H., Kenion, G. B., Church, D. F., Pryor, W. A. (1987). Rates and mechanisms of reaction of nitrogen dioxide with alkenes in solution. *J. Am. Chem. Soc.,* 109, 7059-7063.

Glasson, W. A. (1979). An experimental evaluation of atmospheric nitrosamine formation. *Environ. Sci. Technol.,* 13(9), 1145-1146.

Hanst, P. L., Spence, J. W., Miller, M. (1977). Atmospheric chemistry of N-nitroso dimethylamine. *Environ. Sci. Technol.,* 11(4), 403-405.

Herckes, P., Chang, H., Lee, T., Collett Jr., J. L. (2007). Air pollution processing by radiation fogs. *Water Air Soil Pollut.,* 181, 65-75.

Herrmann, H., Ervens, B., Jacobi, H.-W., Wolke, R., Nowacki, P., Zellner, R. (2000). CAPRAM2.3: A chemical aqueous phase radical mechanism for tropospheric chemistry. *J. Atmos. Chem.,* 36, 231-284.

Hine, J. and Mookerjee, P.K. (1975). The intrinsic hydrophilic character of organic compounds. Correlations in terms of structural contributions. *J. Org. Chem.,*40, 292-298.

Hutchings, J. W.; Ervens, B.; Straub, D.; Herckes, P. N. (2010). Nitrosodimethylamine occurrence, formation, and cycling in clouds and fogs. *Environ. Sci. Technol.,* 41, 393-399.

Karl, M., Gross, A., Leck, C., Pirjola, L. (2007). Intercomparison of dimethylsulfide oxidation mechanisms for the marine boundary layer: Gaseous and particulate sulfur constituents. *J. Geophys. Res.,* 112, D15304, doi:10.1029/2006JD007914.

Karl, M., Wright, R. F., Berglen, T. F., Denby, B. (2011a). Worst case scenario study to assess the environmental impact of amine emissions from a CO_2 capture plant. *Int. J. Greenhouse Gas Control,* 5, 439-447.

Karl, M., Gross, A., Leck, C., Pirjola, L. (2011b). A new flexible multicomponent model for the study of aerosol dynamics in the marine boundary layer. *Tellus,* 63B, 1001-1025.

Karl, M., Dye, C., Schmidbauer, N., Wisthaler, A., Mikoviny, T., D'Anna, B., Müller, M., Clemente, E., Muñoz, A., Porras, R., Ródenas, M., Vázquez, M., Brauers, T. (2012). Study of OH-initiated degradation of 2-aminoethanol. *Atmos. Chem. Phys.,* 12, 1881-1901.

Keefer, L. K. and Roller, P. P. (1973). N-nitrosation by nitrite ion in neutral and basic medium. *Science,* 181, 1245-1247.

Kishore, K., Dey, G. R., Mukherjee, T. (2004). OH radical reactions with ethanolamines: Formation of reducing as well as oxidizing radicals. *Res. Chem. Intermed.,* 30, 837-845.

Kleffmann, J., Kurtenbach, R., Lörzer, J., Wiesen, P., Kalthoff, N., Vogel, B., Vogel, H. (2003). Measured and simulated vertical profiles of nitrous acid. Part I: Field measurements. *Atmos. Environ.,* 37, 2949-2955.

Lammel, G. and Metzig, G. (1998). On the occurrence of nitrite in urban fog water. *Chemosphere,* 374, 1603-1614.

Landgraf, J. and Crutzen, P. J. (1998). An efficient method for online calculations of photolysis and heating rates. *J. Atmos. Sci.,* 55, 863-878.

Lee, C., Yoon, J., von Gunten, U. (2007b). Oxidative degradation of N-nitrosodimethylamine by conventional ozonation and the advanced oxidation process ozone/hydrogen peroxide. *Water Research,* 41, 581-590.

Licht, W. R., Tannenbaum, S. R., Deen, W. M. (1988). Use of ascorbic acid to inhibit nitrosation: kinetic and mass transfer considerations for an in vitro system. *Carcinogenesis,* 9, 365-372.

Lijinsky, W., Keefer, L., Conrad, E., Van de Bogart, R. (1972). Nitrosation of tertiary amines and some biological implications. *J. Natl. Cancer Inst.,* 49(5), 1239-1249.

Lindley, C. R. C., Calvert, J. G., Shaw, J. H. (1979). Rate studies of the reaction of the $(CH_3)_2N$ radical with O_2, NO and NO_2. *Chem. Phys. Lett.,* 67, 57-62.

Marenich, A. V., Olson, R. M., Kelly, C. P., Cramer, C. J. and Truhlar, D. G. (2007) Self-Consistent Reaction Field Model for Aqueous and Nonaqueous Solutions Based on Accurate Polarized Partial Charges. *J. Chem. Theory Comput.,* 3, 2011-2033.

Mäkelä, J. M., Yli-Koivisto, S., Hiltunen, V., Seidl, W., Swietlicki, E., Teinila, K., Sillanpaa, M., Koponen, I. K., Paatero, J., Rosman, K., Hameri, K. (2001). Chemical composition of aerosol during particle formation events in boreal forest. *Tellus,* 53B, 380-393.

Meylan, W. and Howard, P.H. (2000). User's Guide for APOWIN, Version 1.9. Syracuse Research Corporation. North Syracuse, N.Y., March, 2000.

Mezyk, S. P.; Ewing, D.; Kiddle, J. J.; Madden, K. P. (2006). Kinetics and mechanisms of the reactions of hydroxyl radicals and hydrated electrons with nitrosamines and nitramines in water. *J. Phys. Chem. A,* 110, 4732-4737.

Mirvish, S. S. (1975). Formation of N-nitroso compounds: Chemistry, kinetics, and in vivo occurrence. *Toxicology and Applied Pharmacology,* 31, 325-351.

Murphy, S. M., Sorooshian, A., Kroll, J. H., Ng, N. L., Chhabra, P., Tong, C., Surratt, J. D., Knipping, E., Flagan, R. C., Seinfeld, J. H. (2007). Secondary aerosol formation from atmospheric reactions of aliphatic amines. *Atmos. Chem. Phys.,* 7, 2313-2337.

Nielsen, C. J., D'Anna, B., Dye, C., George, C., Graus, M., Hansel, A., Karl, M., King, S., Musabila, M., Müller, M., Schmidbauer, N., Stenstrøm, Y., Wisthaler, A. (2010). Atmospheric Degradation of Amines, Summary Report: Gas phase oxidation of 2-aminoethanol (MEA), CLIMIT project no. 193438, NILU OR 8/2010, Norwegian Institute for Air Research, Kjeller, Norway, available at: http://www.nilu.no, 2010.

Nielsen, C. J., D'Anna, B., Karl, M., Aursnes, M., Boreave, A., Bossi, R., Bunkan, A. J. C., Glasius, M., Hallquist, M., Hansen, A.-M. K., Kristensen, K., Mikoviny, T., Maguta, M. M., Müller, M., Nguyen, Q., Westerlund, J., Salo, K., Skov, H., Stenstrøm, Y., Wisthaler, A. (2011a). Atmospheric Degradation of Amines.

Summary Report: Photo-oxidation of methylamine, dimethylamine and trimethylamine. CLIMIT project no. 201604, NILU OR 2/2011, Norwegian Institute for Air Research, Kjeller, Norway. Available at http://www.nilu.no.

Nielsen, C. J., D'Anna, B., Dye, C., Graus, M., Karl, M., King, S., Musabila, M., Müller, M., Schmidbauer, N., Stenstrøm, Y., Wisthaler, A., Pedersen, S. (2011b). Atmospheric chemistry of 2-aminoethanol (MEA). *Energy Procedia*, 4, 2245-2252.

Platt, U., Perner, D., Harris, G. W., Winer, A. M., Pitts Jr., J. N. (1980). Observations of nitrous acid in an urban atmosphere by differential optical absorption. *Nature*, 285, 312-314.

Plumlee, M.H. and Reinhard, M. (2007). Photochemical attenuation of N-nitrosodimethylamine (NDMA) and other nitrosamines in surface water. *Environ. Sci. Technol.*, 41, 6170-6176.

Salo, K., Westerlund, J., Andersson, P. U., Nielsen, C. J., D'Anna, B., Hallquist, M. (2011). Thermal characterization of alkyl aminium nitrate nanoparticles. *J. Phys. Chem. A*, 115, 11671-11677.

Sander, R. and Crutzen, P. J. (1996). Model study indicating halogen activation and ozone destruction in polluted air masses transported to the sea. *J. Geophys. Res.*, 101, 9121-9138.

Sander, R., Kerkweg, A., Jöckel, P., Lelieveld, J. (2005). Technical note: The new comprehensive atmospheric chemistry module MECCA. *Atmos. Chem. Phys.*, 5, 445–450, doi:10.5194/acp-5-445-2005.

Sander, R., Baumgaertner, A., Gromov, S., Harder, H., J¨ockel, P., Kerkweg, A., Kubistin, D., Regelin, E., Riede, H., Sandu, A., Taraborrelli, D., Tost, H., Xie, Z.-Q. (2011). The atmospheric chemistry box model CAABA/MECCA-3.0. *Geosci. Model Dev.*, 4, 373–380, doi:10.5194/gmd-4-373-2011.

Sander, S. P., Friedl, R. R., Golden, D. M., Kurylo, M. J., Moortgat, G. K., Keller-Rudek, H., Wine, P. H., Ravishankara, A. R., Kolb, C. E., Molina, M. J., Finlayson-Pitts, B. J., Huie, R. E., Orkin, V. L. (2006). Chemical Kinetics and Photochemical Data for Use in Atmospheric Studies, Evaluation Number 15, JPL Publication 06-2, Jet Propulsion Laboratory, Pasadena, CA.

Sandu, A. and Sander, R. (2006). Technical note: Simulating chemical systems in Fortran90 and Matlab with the Kinetic PreProcessor KPP-2.1. *Atmos. Chem. Phys.*, 6, 187–195, doi:10.5194/acp-6-187-2006, 2006.

Sandu, A., Verwer, J. G., Van Loon, M., Carmichael, G. R., Potra, F. A., Dabdub, D., Seinfeld, J. H. (1997). Benchmarking stiff ODE solvers for atmospheric, chemistry problems. 1. Implicit vs explicit. *Atmos. Environ.*, 31, 3151–3166.

Schwartz, S. E. (1983). In: Advances in Environmental Science and Technology. Ed.: Nriagu, J. O., John Wiley and Sons: New York; pp. 1-115.

Schwartz, S. E. (1986). Mass transport considerations pertinent to aqueous phase reactions of gases in liquid water clouds. In: Chemistry of Multiphase Atmospheric Systems, NATO ASI Series, Vol. 6, (ed. W. Jaeschke), Springer, Berlin, 415-471.

Seinfeld, J. H. and Pandis, S. N. (1998). Atmospheric Chemistry and Physics: From Air Pollution to Climate Change. John Wiley and Sons: New York, p. 614.

Siefert, R. L., Johansen, A. M., Hoffmann, M. R. (1998). Measurements of trace metals (Fe, Cu, Mn, Cr) oxidation states in fog and stratus clouds. *J. Air Waste Manage. Assoc.*, 48, 128-143.

Sorooshian, A., Murphy, S. N., Hersey, S., Gates, H., Padro, L. T., Nenes, A., Brechtel, F. J., Jonsson, H., Flagan, R. C. and Seinfeld, J. H. (2008). Comprehensive airborne characterization of aerosol from a major bovine source. *Atmos. Chem. Phys.*, 8, 5489-5520.

Stefan, M.I. and Bolton, J.R. (2002). UV direct photolysis of N-Nitrosodiemthylamine (NDMA): kinetic and product study. *Helvetica Chimica Acta*, 85, 1416-1426.

Tuazon, E. C., Martin, P., Aschmann, S. M., Arey, J., Atkinson, R. (2011). Kinetics of the reactions of OH radicalswith 2-methoxy- 6-(trifluoromethyl)pyridine, diethylamine, and 1,1,3,3,3-pentamethyldisiloxan-1-ol at 298±2 K. *Int. J. Chem. Kint.*, doi 10.1002/kin.20594, 631-638, available online.

Vogel, B., Vogel, H., Kleffmann, J., Kurtenbach, R. (2003). Measured and simulated vertical profiles of nitrous acid - Part II. Model simulations and indications for a photolytic source. *Atmos. Environ.*, 37, 2957-2966.

Weller, C., Tilgner, A., Herrmann, H. (2011). A status on aqueous phase atmospheric chemistry of amines and their degaradation products. Presentation at the CCMWorkshop "Amine emission to air from post combustion CO_2 capture", December 5th and 6th, 2011, 2011, Oslo, Norway.

Wilhelm, E., Battino, R. Wilcock, R. J. (1977). Low-pressure solubility of gases and liquid water. *Chem. Rev.*, 77, 219-262.

Zakharov, I. I., Kolbasin, A. I., Zakharova, O. I., Kravchenko, I. V., Dyshlovoi, V. I. (2008). Quantum-chemical evidence for the possible existence of a new isomer of dinitrogen tetraoxide. *Theoretical and Experimental Chemistry*, Vol. 44, 26-31).

Appendix 1 Henry's law constants

This appendix reports Henrys laws constants calculated as a Variation-Order to the project.

Henry's law constants have been calculated with the SM8 solvation model (Marenich et al., 2007) as it is implemented in the Spartan 08 code. This is a continuum solvation model, utilized in combination with a quantum mechanical representation of the solute. The calculations were carried out at the SM8-M06/6-31+G*level of theory, with the solute geometry optimized with the continuum solvation model. Calculations were carried out for the most stable conformer found for each solute. The model calculates solvation free energies and these are then converted to Henry's law constants. The uncertainty in the calculations is expected to be in around +/-0.5 kcal/mol in solvation energies. Table A1 summarizes the Henry's law constants as computed with the SM8 solvation model.

Table A1: Henry's law constants and solvation energies as computed with solvation model SM8.

	Henry's constant (@298.15 K) mol kg^{-1} atm^{-1}	**dG(Solvation) SM8 kcal mol^{-1}**	**Compound**	**Henry's constant (@298.15 K) mol kg^{-1} atm^{-1}**	**dG(Solvation) SM8 kcal mol^{-1}**
Monomethylamine	84.6	-8.0	DEA-nitramine	$2.37x10^{9}$	-114.7
Dimethylamine	50.5	-4.2	N-nitroso dimethylamine	863	-5.9
Trimethylamine	16.2	-3.5	N-nitroso ethanolamine	$6.36x10^{5}$	-9.8
Monoethanolamine	$4.52x10^{4}$	-8.2	N-nitroso diethanolamine	$1.45x10^{8}$	-13.0
Diethanolamine	$1.26x10^{6}$	-10.2	Isocyanic acid	12.8	-3.4
Triethanolamine	$3.05x10^{4}$	-4.5	Formamide	$3.67x10^{6}$	-10.8
Methylnitramine	$4.78x10^{4}$	-8.3	2-Hydroxy acetamide	$1.10x10^{8}$	-12.8
Dimethylnitramine	$1.99x10^{4}$	-7.7	N-Methyl formamide	$3.03x10^{4}$	-8.0
MEA-nitramine	$4.45x10^{6}$	-10.9	N,N-Dimethyl formamide	$1.85x10^{3}$	-6.3
Piperazine	$1.55x10^{5}$	-9.0	N-nitrososarcosine (deprot)	$5.43 x10^{48}$	-68.3
Nitrosospiperazine	$8.85 x10^{5}$	-10.0	N-nitrososarcosine (prot)	$7.28 x10^{6}$	-11.2
N-nitropiperazine	$2.77 x10^{7}$	-12.0	N-nitrosarcosine (deprot)	$5.43 x10^{48}$	-68.3
N,N' Dinitrosopiperazine	$4.55 x10^{4}$	-8.2	N-nitrosarcosine (prot)	$7.28 x10^{6}$	-11.2
N,N' Dinitropiperazine	$1.08 x10^{4}$	-7.4	N-nitrosoglycine (deprot)	$6.48 x10^{44}$	-62.9
			N-nitroglycine (prot)	$7.18 x10^{42}$	-60.3

Technology for a better society

www.sintef.no